Inorganic Chemistry

Article

pubs.acs.org/IC

Dangling and Hydrolyzed Ligand Arms in [Mn_3] and [Mn_6] Coordination Assemblies: Synthesis, Characterization, and Functional Activity

Krishna Chattopadhyay,[†] Gavin A. Craig,[‡] María José Heras Ojea,[‡] Moumita Pait,[†,§] Animesh Kundu,[†] Junseong Lee,[§] Mark Murrie,[‡] Antonio Frontera,[∥] and Debashis Ray*[,†]

[†]Department of Chemistry, Indian Institute of Technology (IIT), Kharagpur, INDIA

[‡]School of Chemistry, University of Glasgow, Glasgow G12 8QQ,U.K.

[§]Chonnam National University, Gwangju 61186, South Korea

[∥]Departament de Química, Universitat de les Illes Balears, Crta de Valldemossa km 7.5, 07122 Palma de Mallorca (Baleares), SPAIN

Supporting Information

ABSTRACT: Two flexible, branched, and sterically constrained di- and tripodal side arms around a phenol backbone were utilized in ligands H_3L1 and H_5L2 to isolate {Mn_6} and {Mn_3} coordination aggregates. 2,6-Bis{(1-hydroxy-2-methylpropan-2-ylimino)methyl}-4-methylphenol (H_3L1) gave trinuclear complex $[Mn_3(\mu\text{-}H_2L1)_2(\mu_{1,3}\text{-}O_2CCH_3)_4(CH_3OH)_2](ClO_4)_2\cdot 4CH_3OH$ (**1**), whereas 2,6-bis[{1-hydroxy-2-(hydroxymethyl)butan-2-ylimino}methyl]-4-methylphenol (H_5L2) provided hexanuclear complex $[Mn_6(\mu_4\text{-}H_2L2)_2(\mu\text{-}HL3)_2(\mu_3\text{-}OH)_2(\mu_{1,3}\text{-}O_2CC_2H_5)_4](ClO_4)_2\cdot 2H_2O$ (**2**). Binding of acetates and coordination of $\{H_2L1\}^-$ provided a linear $Mn^{III}Mn^{II}Mn^{III}$ arrangement in **1**. A Mn^{III}_6 fused diadamantane-type assembly was obtained in **2** from propionate bridges, coordination of $\{H_2L2\}^{3-}$, and in situ generated $\{HL3\}^{2-}$. The magnetic characterization of **1** and **2** revealed the properties dominated by intramolecular anti-ferromagnetic exchange interactions, and this was confirmed using density functional theory calculations. Complex **1** exhibited field-induced slow magnetic relaxation at 2 K due to the axial anisotropy of Mn^{III} centers. Both the complexes show effective solvent-dependent catechol oxidation toward 3,5-di-*tert*-butylcatechol in air. The catechol oxidation abilities are comparable from two complexes of different nuclearity and structure.

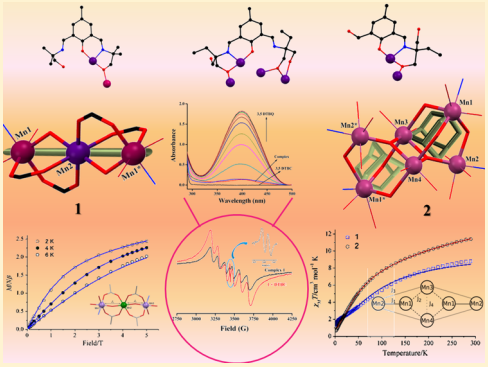

INTRODUCTION

In recent years coordination aggregates of manganese ions have received attention from synthetic point of view due to the involvement of several manganese ions in multinuclear metallocofactors[1] and in the oxygen-evolving center (OEC) of photosystem II in green plants and cyanobacteria.[2−5] OEC contains a unique manganese−calcium−oxo cluster having a separated manganese center. Studies on model compounds provide information during the stepwise growth of trinuclear and higher-order manganese complexes. These complexes can register large ground-state spin (S) values from ferromagnetic exchange interactions and/or spin frustration effects.

Over the years we are interested to develop methodologies for multinuclear manganese complexes of unique structures and spanning range of oxidation states. Discovery of new structural motifs were important because of their similarity in structural mimics, magnetic properties, and as oxidation catalysts.[6−8] Synthesis of such Mn−O clusters often uses trinuclear manganese-carboxylate $[Mn_3O(O_2CMe)_6(py)_3]ClO_4$ as most promising starting material in the presence of variety of in situ generated and/or externally added coordinating groups.[9] Reactions providing higher-nuclearity products of varying oxidation-state combinations and unusual structural motifs, starting from simple metal salts, are of interest in rationalizing the stepwise growth.[10] A renewed interest in manganese complexes of different nuclearity, in N and O donor environment, is evidenced from newer reports of synthesis and reactions.[11−13] For example, a rational pathway can be proposed for the assembly of [Mn_3] and [Mn_6] coordination clusters showing aggregation of unknown type. In this regard the choice of new ligand system is important, which plays role in dictating the final outcome. Alcohol-arm-bearing ligand systems, while coordinating to a particular metal ion center, can show inclination to bridge nearby metal ions through the alkoxido groups. The ancillary ligands like carboxylato and hydroxido groups are versatile for extending the bridging network through coordination from vacant sites around different manganese ions.

Received: November 21, 2016

DOI: 10.1021/acs.inorgchem.6b02813
Inorg. Chem. XXXX, XXX, XXX−XXX

In recent years we and others are working on simple phenol-based Schiff bases to assemble multiple metal ions in a single molecular entity.[14−16] Use of the multiple alcohol-arm-bearing ligand platforms might permit hydroxido/oxido core formation from water following coordination of manganese ions, which in turn could afford products of high nuclearity. Hydroxido/oxido entangled manganese carboxylates are known to exhibit coordination aggregates having new structures and varying oxidation-state combinations involving Mn^{II}, Mn^{III}, and Mn^{IV}. Such aggregates having several metal ion centers in close proximity have shown renewed interests in the field of molecule-based magnets having large ground-state spins.[17−19] Incorporation of Mn^{III} into the aggregates can induce a large magnetic anisotropy for single-molecule magnet (SMM) behavior.[20] Naturally occurring catechol oxidase is the classic example for type 3 copper proteins that is responsible for the catalytic oxidation of a range of *o*-diphenol (catechol) to *o*-quinone. Laboratory prepared complexes of Mn(II/III/IV), Ni(II), and Co(II/III) have been shown to promote such activity, mimicking the above-mentioned biological counterpart, to a greater or smaller extent.[21−23]

Herein we explored the binding potential of H_3L1 and H_5L2 (Scheme 1) to isolate and study new multinuclear manganese

Scheme 1. Two Types of Ligands Having Different Alcohol-Arms

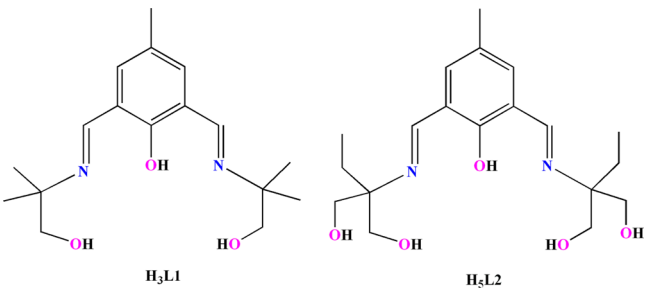

carboxylate and hydroxide aggregates. Simple manganese(II) salts have been used in the presence of different carboxylate ions. Recently we and others have utilized H_3L1 for the synthesis of $[Ni_4]$, $[Ni_6]$,[24] and $[Cu_6]$[25] complexes. The coordination chemistry of H_5L2 is unknown in the literature. This paper reports new $[Mn_3]$ and $[Mn_6]$ complexes $[Mn_3(\mu\text{-}H_2L1)_2(\mu_{1,3}\text{-}O_2CCH_3)_4(CH_3OH)_2](ClO_4)_2\cdot 4(CH_3OH)$ (**1**) and $[Mn_6(\mu_4\text{-}H_2L2)_2(\mu\text{-}HL3)_2(\mu_3\text{-}OH)_2(\mu_{1,3}\text{-}O_2CC_2H_5)_4](ClO_4)_2\cdot 2H_2O$ (**2**), respectively. The former has been assembled via the connections of two ligand-bound mononuclear $\{Mn(H_2L1)\}^{2+}$ fragments by ancillary carboxylate ions and terminal MeOH ligands. In the latter cluster the ligand-bound $\{Mn(H_4L2)\}^{2+}$ units and μ_3-hydroxido-μ-carboxylato bridged trinuclear motifs $[Mn_3(\mu\text{-}OH)(\mu_{1,3}\text{-}O_2CC_2H_5)]$ condense together to result in the isolated cluster. Initial condensation of two $[Mn_3(\mu\text{-}OH)(\mu\text{-}O_2CC_2H_5)]$ units provided a planar $\{Mn_4(\mu_3\text{-}OH)_2(\mu\text{-}O_2CC_2H_5)_4\}$ unit as the backbone on which the fused diadamantane-like $[Mn_6]$ structural motif resulted. Their magnetic exchange interactions involving different metal centers were examined in the solid state, and catalytic activities were also scrutinized in the solution phase.

EXPERIMENTAL SECTION

Materials. The solvents and chemicals used were reagent-grade materials and were purchased from commercial sources like S. D. Fine Chem. Ltd. (India), SRL, E. Merck (India), Sigma-Aldrich (USA), and Alfa Aesar. Without further purification all the chemicals were directly used as received. The sources of the chemicals are as follows: sodium acetate from S. D. Fine Chem (India), propionic acid from E. Merck (India), 2-amino-2-ethylpropane-1,3-diol and 2-amino-2-methylpropan-1-ol from Alfa aesar. 2,6-Diformyl-4-methylphenol was synthesized in gram scale following a modified literature procedure giving improved yield.[26] $Mn(ClO_4)_2\cdot 6H_2O$ was prepared by treating an aqueous perchloric acid (1:1) solution with commercial $MnCO_3$. The sodium propionate was prepared by neutralizing propionic acid (0.15 g, 2.0 mmol) with an equivalent amount of solid NaOH (0.08 g, 2.0 mmol) followed by concentration on a water bath. All other chemical compounds and solvents were reagent-grade materials and were used as received without further purification.

Caution! *Metal complexes of organic ligands with perchlorate counterions are potentially explosive in nature in dry state. Therefore, the material should be prepared in very small amount, and it should be handled with extreme care.*

Synthesis. *H_3L1 (2,6-Bis((1-hydroxy-2-methylpropan-2-ylimino)-methyl)-4-methylphenol).* To a methanol solution (15 mL) containing 2,6-diformyl-4-methylphenol (0.80 g, 5.0 mmol), 2-amino-2-methylpropan-1-ol (0.75g, 10.0 mmol) was mixed by constant stirring. Then the reaction mixture was stirred for about an hour. Several attempts made to separate the solid ligand were unsuccessful. The MeOH solvent is evaporated by using rotatory evaporator to obtain H_3L1 as an oily mass, which was characterized, by Fourier transform infrared (FTIR), ^{1}H NMR, and ^{13}C NMR.

FTIR (cm^{-1}, KBr pellet): 3394(vs), 2974(w), 1635(s), 1061(m), 682(w). ^{1}H NMR (600 MHz, $CDCl_3$, δ ppm): 8.35 (2H, −N=C**H**), 7.24 (2H, aromatic H), 3.49(4H, $-CH_2$), 2.12 (3H, $-CH_3$ attached with benzene ring), 1.17 (12H, $-CH_3$). ^{13}C NMR (150 MHz, $CDCl_3$, δ ppm): 162.03 (imine C), 135.22−124.24 (aromatic C), 71.26 (methylene C attached with oxygen), 60.73 (tertiary C attached to imine N), (26.33−20.04 (methyl C).

H_5L2 (2,6-Bis((1-hydroxy-2-(hydroxymethyl)butan-2-ylimino)-methyl)-4-methylphenol). The H_5L2 was synthesized from Schiff-base condensation reaction of 2,6-diformyl-4-methylphenol (1.0 g, 6.1 mmol) and 2-amino-2-ethyl-propan-1,3-diol (1.3 g, 12.2 mmol) in methanol solvent under stirring condition for 1 h under aerobic condition followed by reflux for 2 h (Scheme S1 in the Supporting Information). The solvent was removed completely by evaporation in air, and an orange oily substance was obtained. The orange color oily substance, H_5L2, was characterized by FTIR and NMR spectroscopy. Major ^{1}H NMR peaks confirm the ligand formation. The ligand was used directly for complexation reactions without further purification.

FTIR (cm^{-1}, KBr pellet): 3421(vs), 1636(s), 1054(w), 619(w). ^{1}H NMR (600 MHz, $CDCl_3$, ppm): 8.345 (2H, −N=C**H**), 7.34−7.28 (2H, aromatic H), 3.35 (8H, $-OCH_2$), 2.22 (3H, $-CH_3$ substituent on phenyl ring) 1.61 (4H, $-CH_2$), 0.86 (6H, $-CH_3$). ^{13}C NMR (150 MHz, $CDCl_3$, ppm): 165.41 (imine C), 161.61−125.25 (aromatic C), 65.31 (methylene C attached with oxygen), 64.7 (tertiary C attached to immine N), 25.04 (methyl C attached with benzene ring), 20.40 (methelene C), 7.29 (methyl C).

*$[Mn_3(\mu\text{-}H_2L1)_2(\mu_{1,3}\text{-}O_2CCH_3)_4(CH_3OH)_2](ClO_4)_2\cdot 4CH_3OH$ (**1**).* To an MeOH solution (10 mL) of H_3L1 (1 mmol, 0.31 g) in a conical flask, 2 mmol (0.72 g) $Mn(ClO_4)_2\cdot 6H_2O$ was added under constant stirring. After 15 min of stirring, sodium acetate (2 mmol, 0.16 g) was added to it. The solution became brown in color. The entire mixture was then refluxed for about an hour. After that, the solution was filtered and kept for slow evaporation. Brown crystalline solid was obtained on slow evaporation of the solvent. The compound was then recrystallized from MeOH−MeCN mixture (1:1), and nice brown crystals suitable for single-crystal X-ray diffraction were obtained after one week. Yield: 0.59 g, 63%. Anal. Calcd for $C_{48}H_{82}Cl_2Mn_3N_4O_{28}$ (1398.86 g mol^{-1}): C, 41.21; H, 5.91; N, 4.01. Found: C, 41.16; H, 5.85; N, 3.90%. Selected FTIR bands (KBr, cm^{-1}): 3421(broad), 1658(strong), 1603(strong), 1549(strong), 1405(medium), 1090(medium). Molar

DOI: 10.1021/acs.inorgchem.6b02813
Inorg. Chem. XXXX, XXX, XXX−XXX

Scheme 2. Synthetic Routes to Complexes 1 and 2

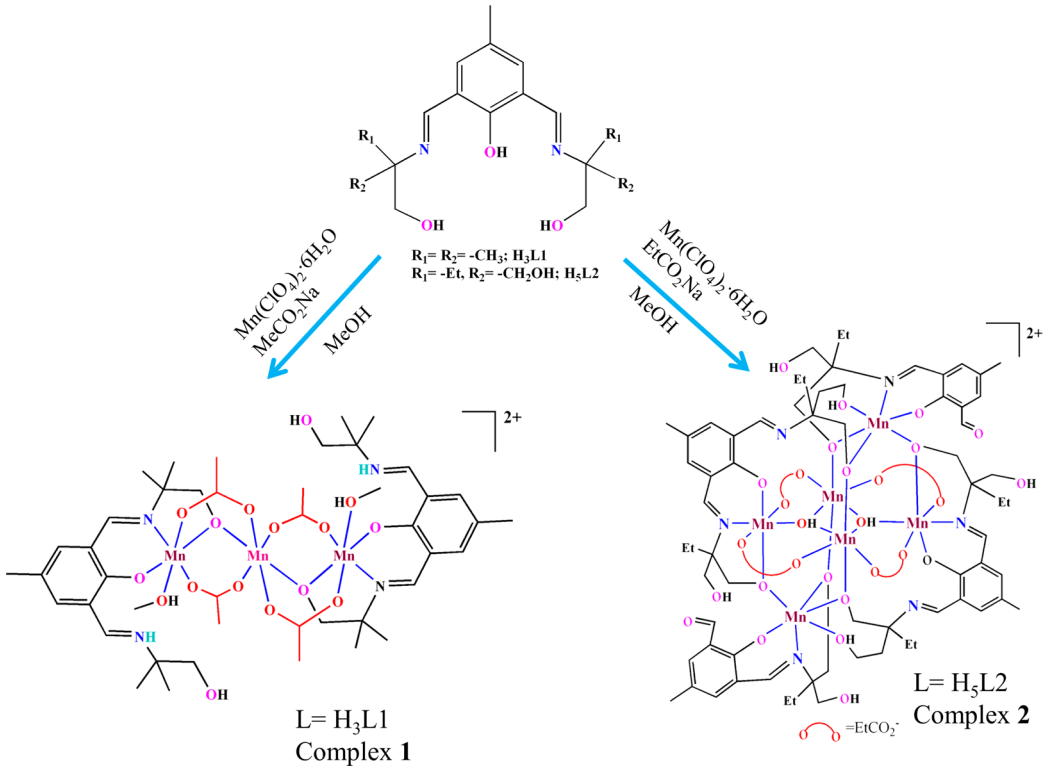

conductance, Λ_M (methanol solution, Ω^{-1} cm^2 mol^{-1}): 164.2. UV–Vis spectra [λ_{max}, nm (ε, L mol^{-1} cm^{-1})] (MeCN solvent): 586 (110), 399 (16 200), 255 (54 240).

[Mn$_6$(μ_4-H$_2$L2)$_2$(μ-HL3)$_2$(μ_3-OH)$_2$($\mu_{1,3}$-O$_2$CC$_2$H$_5$)$_4$](ClO$_4$)$_2$·2H$_2$O (**2**). An MeOH solution (15 mL) of Mn(ClO$_4$)$_2$·6H$_2$O (0.90 g, 2.5 mmol) was added dropwise during 10 min to a methanol (10 mL) solution of H$_5$L2 (0.37 g, 1.0 mmol) under constant stirring. The solution color was changed to wine red. After 15 min sodium propionate (2 mmol, 0.20 g) salt was added to the reaction mixture when solution color changed to dark brown. The reaction mixture was further stirred for 2 h. After that the solution was filtered, and slow evaporation of the solvent at ambient condition gave brown block-type crystals suitable for X-ray diffraction after 12 d. Yield: 1.40 g, 65%. Anal. Calcd for C$_{78}$H$_{110}$Cl$_2$Mn$_6$N$_6$O$_{38}$ (2140.26 g mol^{-1}): C, 43.77; H, 5.18; N, 3.93. Found: C, 43.52; H, 5.13; N, 4.02%. Selected FTIR bands (KBr, cm^{-1}): 3404(broad), 2967(medium), 1645(s), 1620-(strong), 1577(strong), 1547(strong), 1454(medium), 1140-(medium), 1115(medium), 1078(strong), 621(medium). Molar conductance, Λ_M (methanol solution, Ω^{-1} cm^2 mol^{-1}): 182.4. UV–Vis spectra [λ_{max}, nm (ε, L mol^{-1} cm^{-1})] (MeCN solvent): 586 (170), 410 (27 200), 264 (94 557).

Physical Measurements. The purity of the complexes was examined by measuring the percentage of carbon, hydrogen, nitrogen with a PerkinElmer model 240C elemental analyzer. A Shimadzu UV–vis–NIR spectro-photometer model UV 3100 was used for recording the solution-state electronic absorption spectra of the compounds. A PerkinElmer FTIR spectrometer model RX1 was used to obtain the FTIR spectra on KBr pellets. The high-resolution mass spectra (HRMS) of the compounds were recorded in electrospray ionization (ESI) mode using a Bruker esquire 3000 plus mass spectrometer. The electrical conductivity of the compounds was measured in methanol solvent by a Unitech type U131C digital conductivity meter with a solute concentration of ~1 × 10^{-3} M. The powder X-ray diffraction patterns of the powder compounds were recorded by using a Bruker AXS X-ray diffractometer (40 kV, 20 mA) with Cu Kα radiation (λ = 1.5418 Å) with an angular range of (2θ) of 5–50°. Electron paramagnetic resonance (EPR) spectra were recorded at 9.13 GHz (X-band) in continuous wave mode with a Bruker ELEXSYS 580 X-band EPR spectrometer equipped with a standard accessory for room temperature operation (298 K).

Magnetic Measurements. Direct-current (dc) and alternating-current (ac) magnetic measurements were performed on polycrystalline samples of compounds **1** and **2** constrained in eicosane, using a Quantum Design SQUID magnetometer furnished with a 5 T magnet in the School of Chemistry at the University of Glasgow. The dc measurements were performed in the temperature range of 290–1.8 K under an applied field of 1000 Oe. Field-dependent magnetization measurements were performed at 2, 4, and 6 K, over the range of 0–5 T. Dynamic susceptibility measurements were performed over the temperature range of 2–10 K, with a drive field of 3 Oe, and a frequency range from 1 to 1488 Hz. Data were corrected for the diamagnetism of the compound through the approximation that χ_{DIA} ≈ 0.5 × MW × 1 × 10^{-6} cm^3 mol^{-1} (MW = molecular weight), and for the diamagnetic contributions of the sample holder and eicosane through measurements.

Method for Kinetic Study. The catecholase activity of the complexes were studied in MeOH and MeCN separately using 3,5-di-*tert*-butylcatechol (3,5-DTBCH$_2$) as the model substrate. The oxidation of 3,5-DTBCH$_2$ to 3,5-di-*tert*-butylquinone (3,5-DTBQ) was followed on a Shimadzu UV 3100 UV–vis–NIR spectro-photometer. The reactions were monitored at the quinone band maxima at ~400 nm. Kinetic experiments were performed in MeOH and MeCN medium, and different reaction sets were examined using constant concentration (~1.0 × 10^{-5} M) of complexes and varying amount of 3,5-DTBCH$_2$ (10 to 100 equiv); the spectral changes were monitored with time at band maxima of quinone. The initial rates for each catalyst–substrate combination were calculated from the slope of the absorbance versus time plot. Kinetic analyses were executed following the Michaelis–Menten method, and important kinetic parameters were derived from the Lineweaver–Burk plots.

Crystal Structure Determination. Suitable single crystals of **1** and **2** were chosen for X-ray diffraction, and the data were collected on a Bruker SMART APEX-II CCD X-ray diffractometer, which is furnished with a graphite-monochromated Mo Kα (λ = 0.710 73 Å) radiation by the ω-scan method at 293 K (100 K, for **1**) with a counting time of 4 s per frame. Data integration, reduction, and space

DOI: 10.1021/acs.inorgchem.6b02813
Inorg. Chem. XXXX, XXX, XXX–XXX

Scheme 3. Coordination-Induced Partial Hydrolysis of H_5L2 to H_3L3

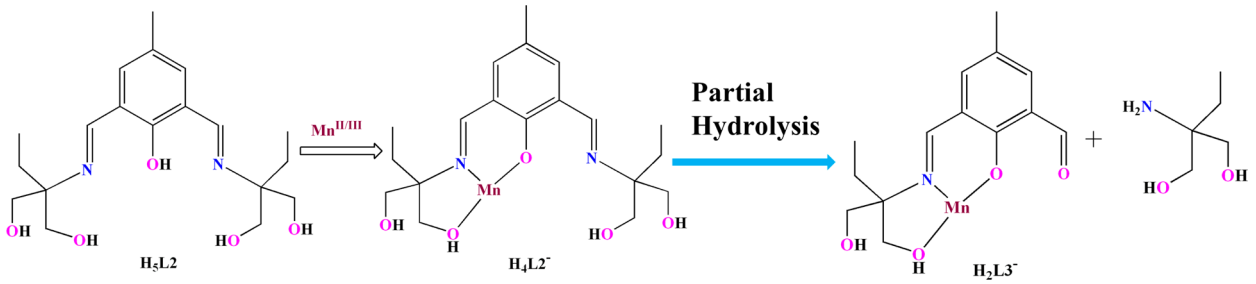

group determination were performed using XPREP and SAINT software.[27] The structures were solved using the direct method through the SHELXS-97[28] and refined by SHELXL-97[29] program package associated with WINGX system Version 1.80.05.[30] The locations of the heaviest atoms (Mn) were determined easily, and the O, N, and C atoms were then fixed from the difference Fourier maps. Anisotropic refinement was performed for the non-hydrogen atoms. H atoms were incorporated in calculated positions and refined using fixed geometry and riding thermal parameters. All the crystallographic diagrams were generated using Diamond[31] and POV-ray[32] software. Information regarding the X-ray diffraction data collection and structure refinements of the compounds is provided in Table S1. CCDC Nos. 1517620 and 1517621 contain the supplementary crystallographic data of the two compounds.

Theoretical Methods. The magnetic properties of the two compounds were calculated employing density functional theory (DFT) in combination with the broken symmetry approach[33−35] with the help of Gaussian 09 package.[36] This study used B3LYP/6-31G* level of theory, which is a good agreement between the size of the systems and the computational demands. The crystallographic coordinates where the positions of the hydrogens were optimized, were used for these calculations. Moreover, the theoretical models were simplified using H atoms instead of methyl groups in the ligand.

For the linear trinuclear system Mn(III)−Mn(II)−Mn(III) **1**, we have a strictly symmetric system in which two of the terminal magnetic centers (Mn1 and Mn1*; see Figure 1 for labeling scheme) are related to a symmetry element that passes across the third one (Mn2). Therefore, we can conclude that $J_{12} = J_{21*} = J$ with a consequent simplification of the calculations.[37,38] Further, the interaction between Mn1 and Mn1* can be neglected taking into account the large separation of the two Mn(III) metal centers at two ends. Therefore, the magnetic coupling constant of compound **1** can be obtained using the energy of only two states. For the calculations of the hexanuclear complex **2**, we evaluated each individual coupling constant (J_1 to J_4) using the methodology proposed by Alvarez group[39,40] in mutinuclear systems. This method consists of substituting paramagnetic atoms by diamagnetic ones to reduce the evaluation of coupling constants to calculations for magnetically dinuclear complexes. This strategy is very convenient and accurate to estimate each individual coupling constant.

RESULTS AND DISCUSSION

Synthetic Concerns. H_3L1 and H_5L2 were examined for their ability to trap multiple metal ions in $[Mn_3]$ (**1**) and $[Mn_6]$ (**2**) aggregates (Scheme 2). Reaction of H_3L1 with $Mn(ClO_4)_2\cdot 6H_2O$ and CH_3CO_2Na in 1:2:2 molar ratio in MeOH and in absence of any added base in air resulted **1**. Oxygen of air was consumed for partial oxidation of terminal Mn^{II} centers to Mn^{III} in **1** (vide supra). The course of the reaction followed by the crystallization for **1** is summarized in eq 1 below.

$$2H_3L1 + 3Mn(ClO_4)_2\cdot 6H_2O + 4CH_3CO_2Na + (1/2)O_2 \xrightarrow{MeOH} [\text{brown crystalline material}] \xrightarrow{MeOH-MeCN} [Mn^{III}_2Mn^{II}(H_2L1)_2(\mu_{1,3}\text{-}O_2CCH_3)_4(CH_3OH)_2](ClO_4)_2\cdot 4CH_3OH \quad (1)$$

During the formation of **1** in solution, two deprotonated $\{H_2L1\}^-$ gave two $\{Mn^{III}(H_2L1)(O_2CCH_3)(H_2O)_2\}^+$ units for the trapping of in situ generated $\{Mn^{II}(O_2CCH_3)_2\}$ in the reaction medium. Thus, the molecular structure of **1** is composed of two ligand-bound terminal Mn^{III} centers connected by a central ligand-free Mn^{II} unit through the alkoxido bridges of ligand and oxygen connectors of carboxylate anions (vide supra).

Interestingly reaction of H_5L2 with $Mn(ClO_4)_2\cdot 6H_2O$ and $C_2H_5CO_2Na$ in lieu of CH_3CO_2Na as used in the previous case and in 1:2.5:2 molar ratio in MeOH resulted in **2** in 65% yield. Direct reaction of the components in MeOH solution leads to brown powdered complex, which, on recrystallization from MeOH−MeCN mixture (1:1), gave brown crystals. Several reactant stoichiometries were tried before the above-mentioned molar ratio was settled. The course of reaction for the formation of **2** is given below.

$$4H_5L2 + 6Mn(ClO_4)_2\cdot 6H_2O + 10C_2H_5CO_2Na + (3/2)O_2 \xrightarrow{MeOH} [Mn^{III}_6(H_2L2)_2(HL3)_2(\mu_3\text{-}OH)_2(\mu_{1,3}\text{-}O_2CC_2H_5)_4](ClO_4)_2\cdot 2H_2O + 10NaClO_4 + 6C_2H_5CO_2H + 35H_2O \quad (2)$$

During the complexation reaction under aerobic conditions, the Mn(II) ions from the perchlorate salt undergo aerial oxidation leading to the entrapment of Mn(III) in the final product, **2**. Metal ion coordination induced partial hydrolysis generates hydrolyzed ligand H_3L3 (Scheme 3) and gives stability to the final isolable species.

Hydrolysis of imine arms by solvent/bases to produce 2-aminoethanol in the reaction medium is well-known.[41] Steric crowding on the α-carbon to the amine function further facilitates the removal of substituted 2-aminoethanol group following oxidation of Mn^{II} center to Mn^{III} and coordination within ONO tridentate pocket of $\{HL3\}^{2-}$. The removed bis(hydroxymethyl) amine, capable of bridging multiple metal ions in free form, was not suitable under these reaction conditions to show coordination or chelation. Both the complexes were characterized by FTIR (Figure S1) and electronic spectral measurements (see Supporting Information). The phase purity of the complexes is confirmed by powder X-ray diffraction (PXRD) studies. The experimental PXRD patterns (Figure S2) are in good agreement with the simulated ones obtained from single-crystal XRD data.

Structural Description. **$[Mn_3(\mu\text{-}H_2L1)_2(\mu_{1,3}\text{-}O_2CCH_3)_4(CH_3OH)_2](ClO_4)_2\cdot 4CH_3OH$ (1).** Compound **1** crystallizes in the triclinic crystal system and $P\bar{1}$ space group. The perspective view of the mixed valence trinuclear cationic unit is shown in Figure 1.

Complex **1** has a linear trinuclear structure with the central Mn^{II} ion at the inversion center. Each $\{HL1\}^{2-}$ anion derived from H_3L1 ligand provides tridentate ONO meridional

DOI: 10.1021/acs.inorgchem.6b02813
Inorg. Chem. XXXX, XXX, XXX−XXX

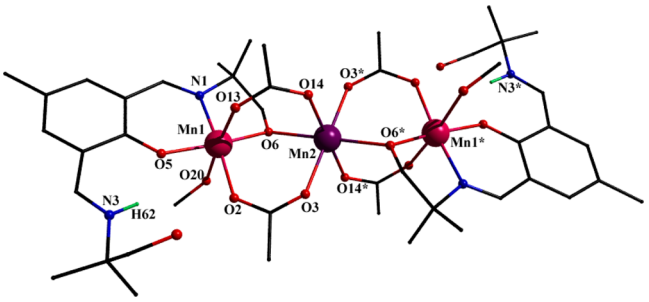

Figure 1. View of the complex unit in **1** with partial atom numbering scheme. Counter ions and solvent molecules in the lattice are omitted for clarity. H atoms are shown only for the protonated imine group. Color code: C black, N blue, O red, Mn^{II} purple, Mn^{III} pink.

coordination to terminal Mn^{III} ions (Mn1 and Mn1*). The deprotonated alkoxido ions of ligand arms from two ligands bridge the central Mn^{II} ion (Mn2). The second pockets of the ligands remain vacant, and the imine N is protonated in zwitterionic form (Chart I).

Chart I. Coordination Zwitterionic H_3L1

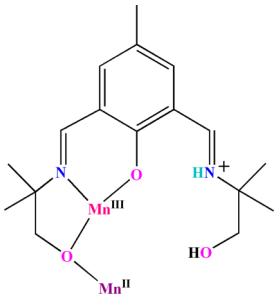

Two ligand-bound terminal $\{Mn^{III}(L1)\}^{2+}$ units are connected to the central Mn^{II} ion by the alkoxido ligand ends (O6 and O6*) and two exogenous acetate groups (Figure S3).

The core structure of **1** (Figure 2) elaborates the coordination connectivity, disposition of donor atoms, and

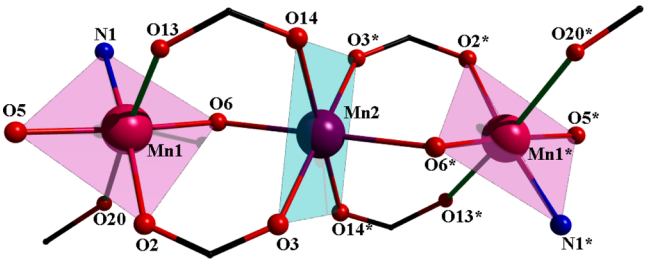

Figure 2. Core view of **1**. Color code: C, black; N, blue; O, red; Mn^{II}, purple; Mn^{III}, pink.

arrangement of the three manganese ions sitting within distorted octahedral geometry. Careful scrutiny of the bond distances (Table S2) around the terminal Mn ions (Mn1 and Mn1*) revealed them as Mn^{III} centers, whereas the central Mn ion is assigned to Mn^{II} center. These oxidation states were further verified by a bond valence sum (BVS) analysis.[42] The bond valence model is a popular method in coordination clusters to estimate the oxidation states of the metal ions present in the aggregate.[43] The results of bond valence sums are summarized in Table S4 of Supporting Information. The tridentate ONO (O5N1O6 or O5*N1*O6*) bite of the ligand along with the carboxylate O2 (or O2*) forms the NO3 basal plane. For Mn^{III} ions (Mn1 and Mn1*) the Mn−X [X = N or O] bond distances along this basal plane varies from 1.867(3) to 1.992(4) Å. The axial donor atoms from one carboxylate oxygen (O13 or O13*) and methanol oxygen (O20 or O20*) remain at 2.183(4) and 2.270(4) Å. The central Mn^{II} ion (Mn2) records Mn−O bond distances in the range of 2.130(4)−2.147(3) Å along the basal plane and 2.193(4) Å along apical direction. Interestingly four acetato groups in $\mu_{1,3}$ bridging mode clearly established the basal−basal (O2−O3 and O2*−O3*) and apical−basal (O13−O14 and O13*−O14*) connectivity.

The terminal phenoxido oxygen atom provides a six-membered chelate bite to the manganese ions giving Mn^{III}−O separations of 1.900(3) Å, whereas the alkoxido end gives a five-membered chelate bite as well as extending bridging connectivity to the central Mn^{II} ion. In this regard, oxygen atoms make Mn^{III}−O bonds of 1.867(3) Å and Mn^{II}−O bond of 2.147(3) Å.

The lattice-trapped solvent MeOH molecules serve as good hydrogen-bond donors (D) to two of the carboxylate acceptors (A) involved in bridging. The protonated imine group (D) is also involved in hydrogen-bonding interactions with the phenoxido oxygen (A). Such intramolecular interactions impart added stabilization to the trinuclear structure (Figure S4). The D···A separations for O···O contacts vary from 2.781(7) to 2.787(5) Å, whereas that distance for N···O contacts is 2.674(5) Å. The D−H···A angles range from 115 to 165° (Table S3).

$[Mn_6(\mu_4\text{-}H_2L2)_2(\mu\text{-}HL3)_2(\mu_3\text{-}OH)_2(\mu_{1,3}\text{-}O_2CC_2H_5)_4](ClO_4)_2\cdot 2H_2O$. Complex **2** crystallizes in the monoclinic $C2/c$ space group, and the crystal data are summarized in Table S1. Significant bond distances and bond angles are listed in Table S2. The typical hexametallic pattern formed from binding of two each of two types of ligand system for **2** is shown in Figure 3. The molecule is symmetric with respect to a twofold rotational axis of symmetry ($-x$, y, $1/2 - z$), and half of the molecule constitutes the asymmetric unit.

The entire structure of **2** is grown on two H_2L2^{3-} groups and two of its hydrolyzed congener $HL3^{2-}$. Each H_2L2^{3-} shows a characteristic coordination mode to four different Mn centers through one imine N, one nonbridging phenoxido O, two bridging alkoxido O atoms, and one terminal OH group. Two

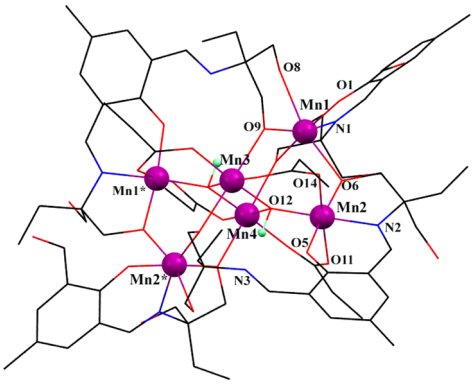

Figure 3. View of the complex unit in **2** with partial atom numbering. Counter ions are omitted for clarity. H atoms are shown only for μ_3-OH groups. Color code: C, black; H, pale green; Mn, purple; N, blue; O, red.

DOI: 10.1021/acs.inorgchem.6b02813
Inorg. Chem. XXXX, XXX, XXX−XXX

single-arm hydrolyzed ligands ($HL3^{2-}$) show a special type of coordination mode to two manganese ions through one imine N, one nonbridging phenoxido O, and one bridging alkoxido O atom (Chart II). The O atom of the −CHO group originating

Chart II. Unusual Coordination Modes of H_5L2 and H_3L3

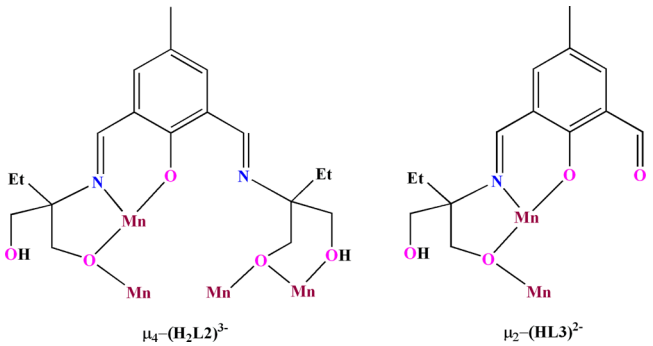

from hydrolysis remained as a pendant group without showing any kind of bonding to the manganese centers. Unlike the liberated 2-amino-2-ethylpropan-1,3-diol in the present case, the removed 2-amino-2-methyl-1-propanol has been shown to stabilize nickel-based multimetallic aggregates.[44] (Figure S5).

The six manganese centers are linked via two μ_3-OH groups and four μ-O_2CR exogenous bridges. This hydroxido-carboxylato core is surrounded by four ligand units of two types (Figure 3). The hydroxido groups obtained from the solvent water molecules were crucial for the formation of $\{Mn^{III}_4(\mu_3\text{-OH})_2\}$ type of butterfly unit from fusion of two triangular subunits $\{Mn^{III}_3(\mu_3\text{-OH})\}$.[45−47] The Mn−O distances within this core range from 1.876(4) to 2.250(4) Å. Within this butterfly unit the O12 and O12* atoms connect Mn2, Mn2*, Mn3, and Mn4. The fifth and sixth manganese centers (Mn1 and Mn1*) sit on two sides of the triangular bases to provide the hitherto unknown fused-diadamentane structure in manganese carboxylate chemistry (Figure 4). Two μ_3-OH groups (O12 and O12*) lie 0.125 Å above and below the mean Mn_4 plane consisting of Mn2, Mn2*, Mn3, and Mn4. In this structure the fifth and sixth Mn^{III} ions (Mn1 and Mn1*) remain at 3.053 Å apart from this plane. This recorded a separation of 3.181(5) Å for O12−Mn1 and O12*−Mn1*. This long separation thus prevented the possibility for further deprotonation from μ_3-OH groups and resulting in the formation of a $\{Mn_4(\mu_4\text{-O})\}$ complex as seen in Cu^{II}-carboxylate chemistry.[48,49] Within the $\{Mn_4(\mu_3\text{-OH})_2\}$ butterfly core the Mn3···Mn4 separation is shortest at 2.820 Å compared to known reports for triangular fragments.[50] The other manganese centers are separated from each other by the distances falling in the range from 3.414 to 3.647 Å (Figure S6). For oxido-bridged $\{Mn^{III}_3(\mu_3\text{-O})\}$ fragments the Mn···Mn separations remain in the range of 3.143−3.414 Å,[51] and for complexes containing $\{Mn_4(\mu_4\text{-O})\}$ cores the Mn···Mn distances range from 3.122 to 3.629 Å.[52]

Four manganese ions (Mn1, Mn1*, Mn2, and Mn2*) have primary coordination from the anionic ligand part or its hydrolyzed congener. This has been evidenced from the four Mn−N bonds, from the imine N atoms, within 2.008(6) to 2.018(6) Å. The other two manganese ions (Mn3 and Mn4) did not show any primary coordination to ligand systems except hydroxido, carboxylato, alkoxido, and alcohol coordination in the 1.876(4) to 2.250(4) Å range. Among these, alcohol O atoms showed longest distances, and phenoxido O atoms register shortest within this group. The fused-diadamentane structure has a unique $[Mn_6(OH)_2O_6]$ core (Figure 5) hitherto

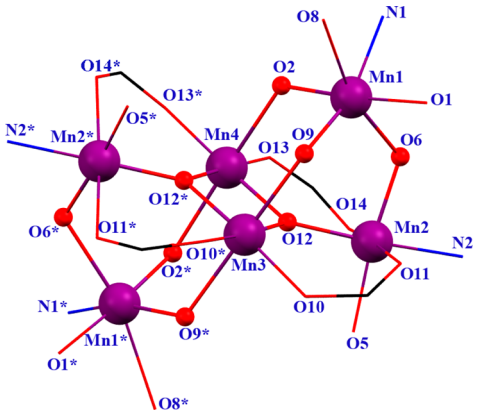

Figure 5. Core view of **2**. Color code: C, black; Mn, purple; O, red; N. blue.

unknown in the literature. The bond valence model was used to analyze the number of electrons each atom contributes to the coordinate bonds formed. The BVS calculations (Table S4) assigned the oxidation state to all manganese ions as Mn^{III}. In distorted octahedral environments two types of manganese centers are present in this complex, namely, $[MnO_5N]$ and $[MnO_6]$. Two (Mn1, Mn1*) and four (Mn2, Mn2*) different

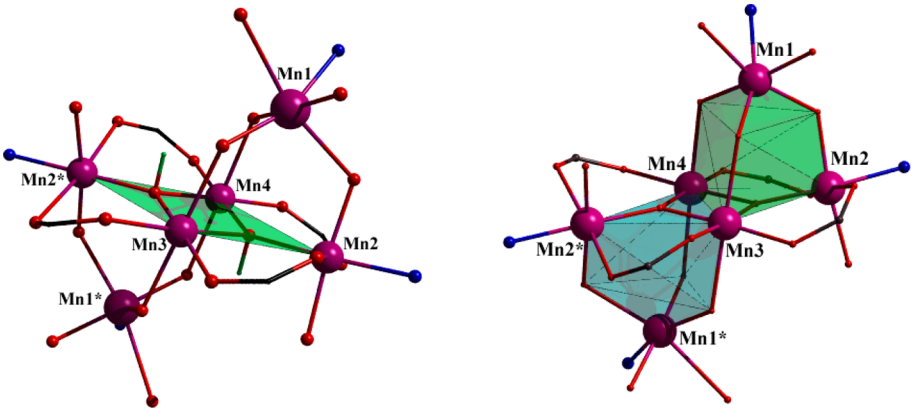

Figure 4. Fused diadamantane-like arrangement in **2**.

DOI: 10.1021/acs.inorgchem.6b02813
Inorg. Chem. XXXX, XXX, XXX−XXX

Mn−O bonds were seen with the [MnO_5N] type, and the [MnO_5N] type showed three different types of Mn−O bonds (Table 1).

Table 1. Types of Mn−O and Mn−N Bonds in 2

coordination environment	metal ions	donor atoms	bond distances (Å)
[MnO_5N]	Mn1 and Mn1*	Mn−O(phenoxido)	1.889(5)
		Mn−O(alkoxido)	1.884(5)−2.420(5)
		Mn−N(imine)	2.018(6)
[MnO_5N]	Mn2 and Mn2*	Mn−O(phenoxido)	1.931(4)
		Mn−O(hydroxido)	1.886(4)
		Mn−O(alkoxido)	1.876(4)
		Mn−O(carboxylato)	2.193(5)−2.213(5)
		Mn−N(imine)	2.008(6)
[MnO_6]	Mn3 and Mn4	Mn−O(hydroxido)	1.876(4)
		Mn−O(alkoxido)	2.241(4)−2.250(4)
		Mn−O(carboxylato)	1.958(5)−1.959(5)

Each H_3L2^{2-} and $HL3^{2-}$ has one dangling alcohol group not bound to any metal ions and actively participates in hydrogen-bonding interactions. They form intermolecular hydrogen bonds with two lattice trapped water molecules resulting in an infinite three-dimensional (3D) network (Figure S7). The characteristic hydrogen-bonding parameters are listed in Table S3. The perchlorate counteranions are trapped within this H-bonded 3D network. The D···A distances vary from 2.746(15) to 3.313(15) Å, and the D−H···A angles range from 110 to 157°.

Magnetic Properties. The temperature dependence of the molar magnetic susceptibility χ_M of compounds **1** and **2** was measured under a magnetic field of 0.1 T over the temperature range of 290−1.8 K (Figure 6). At 290 K, the values of $\chi_M T$ for

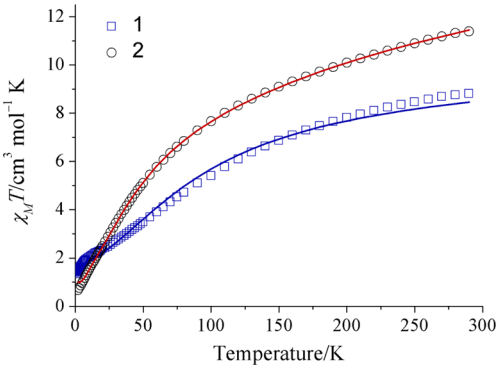

Figure 6. Plots of $\chi_M T$ vs T for **1** and **2**. The solid lines correspond to fits of the data (see text for details).

1 and **2** are 8.80 and 11.40 cm^3 mol^{-1} K, respectively. These values are significantly below that expected theoretically for the compounds (10.38 cm^3 mol^{-1} K for **1** and 18.00 cm^3 mol^{-1} K for **2**, assuming g = 2.0 in both cases), consistent with dominant intramolecular anti-ferromagnetic exchange interactions. On decreasing the temperature, $\chi_M T$ decreases continually for both the compounds. Below 20 K, a small plateau is observed in $\chi_M T$ for **1**, before a final, sharp decrease to 1.34 cm^3 mol^{-1} K at 1.8 K. Compound **2** presents a continual decrease in $\chi_M T$ reaching a minimum value of 0.66 cm^3 mol^{-1} K at 2.0 K. Field-dependent magnetization measurements were performed for compound **1** at 2, 4, and 6 K (Figure 7). The magnetization does not saturate at the highest measured field of 5 T, indicating the presence of magnetic anisotropy arising from the Mn(III) ions.

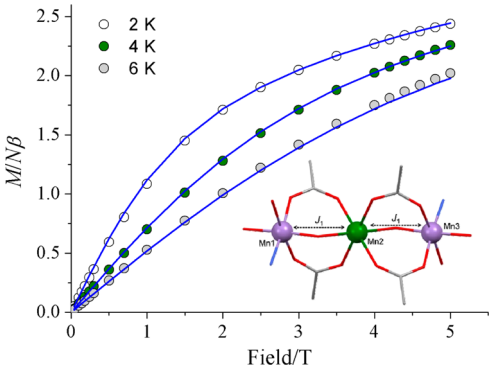

Figure 7. Plots of M vs H for **1**. The solid lines correspond to the fit of the data (see text for details). (inset) The model considered.

The magnetic data for **1** and **2** were fitted using the program Phi 2.0.[53] For compound **1**, it was possible to simultaneously fit both the $\chi_M T$ and magnetization data. One coupling constant, J_1, was considered between the outer Mn(III) ions and the central Mn(II) ion (see inset of Figure 7), and the g-value was fixed at 2.0. Any possible exchange interaction between the outer Mn(III) ions was neglected, based on previous studies.[54,55] The single-ion axial zero-field splitting parameter d was included in the fit for both Mn(III) ions. An intermolecular interaction zJ' of 0.02 cm^{-1} and a temperature-independent paramagnetism (TIP) contribution of 3.2 × 10^{-6} cm^3 mol^{-1} were also included.[56] The Hamiltonian used was as follows

$$\hat{\mathcal{H}} = -2\mathcal{J}_1(\hat{S}_1\hat{S}_2 + \hat{S}_2\hat{S}_3) + g\mu_B\vec{B}\sum_{i=1}^{3}\vec{s}_i + d_1\left(\hat{S}_{1z}^2 - \frac{1}{3}S_1(S_1+1)\right) + d_3\left(\hat{S}_{3z}^2 - \frac{1}{3}S_3(S_3+1)\right) \quad (3)$$

and the results of the fit are shown as solid lines in Figures 6 and 7. The fitting process yielded a value of J_1 = −5.95 cm^{-1} and a value of d_i for each Mn(III) ion of −2.25 cm^{-1} (R = 97%). These results are consistent with the relatively large Mn−O−Mn angle (120.37(14)°) bridging the Mn(III) and Mn(II) ions and with the observed tendency of acetate-bridged {$Mn^{III}_2Mn^{II}$} complexes to display anti-ferromagnetic coupling.[57] The tetragonal elongation around the Mn(III) ions is conducive to negative values of d_i.[58]

Given the axial anisotropy of the Mn(III) ions determined by the dc magnetic studies for **1**, ac susceptibility measurements were performed to ascertain whether the complex displays slow relaxation of the magnetization. In zero dc field, no out-of-phase component to the susceptibility χ'' was observed (Figure S8). Application of a static field of H = 2000 Oe was shown to allow measurement of the onset of slow magnetic relaxation at 2 K. A subsequent field sweep at 2 K showed that applied fields as low as 500 Oe were sufficient to bring about an appreciable component to the out-of-phase susceptibility (Figure S9); however, any maxima were beyond the frequency range of the magnetometer, and the data were not analyzed further.

DOI: 10.1021/acs.inorgchem.6b02813
Inorg. Chem. XXXX, XXX, XXX−XXX

We also used DFT calculations using the broken symmetry approach to estimate the magnetic coupling constant J in **1** using the crystallographic coordinates. The theoretical value of J (-6.07 cm^{-1}) calculated at the B3LYP/6-31G* level of theory is in excellent agreement with the experimental value (-5.95 cm^{-1}) and confirms the anti-ferromagnetic coupling. With an aim to investigate mechanism for the magnetic exchange coupling, the spin density distribution was analyzed. The atomic spin population values on the Mn metal centers and the donor atoms of the ligands are listed in Table S5. The Mulliken spin population analysis for the high-spin (HS) configuration shows that some spin (ca. 0.38 e) is delocalized through the ligands, and the rest (12.62 e) is supported by the Mn ions. The representation of the spin distributions relating to one of the "broken-symmetry" wave function and the high-spin states for complex **1** are described in Figure 8, where α and β spin states

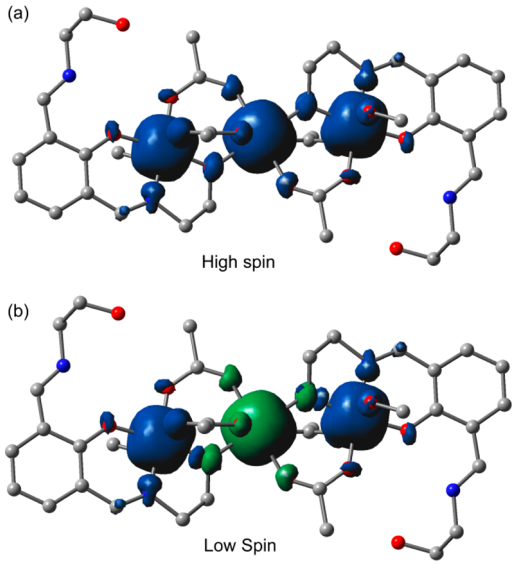

Figure 8. Graphical representation of spin density (contour 0.004 e Å^{-3}) at the high spin (a) and low spin (b) configurations of complex **1**.

are denoted by positive (blue) and negative (green) signs, respectively. The broken-symmetry spin population values of +3.84 on Mn(III) and −4.81 on Mn(II) confirms the centers to be magnetic centers and that the spin delocalization is modest (~2.7% of the spin arising from the unpaired electrons on the Mn^{II}/Mn^{III} centers is delocalized to the ligand framework). The spin population on the donor atoms have the same sign as that of the Mn atoms to which they are bonded (see Table S5). Remarkably, the spin on the acetate O atoms (O13/O14) is ca. 0.08 e in the HS state and −0.01 e in the broken-symmetry state of complex **1**. In contrast the spin density is almost negligible on the alkoxide atoms. Consequently, the bridging oxygens of acetate are more effective in mediating the magnetic exchange.

Compound **2** contains two edge-sharing tetrahedra of Mn(III) ions, with Mn1 sitting above a basal-plane formed by Mn2, Mn3, and Mn4, with the latter two ions forming the shared edge. To fit the data, four different coupling constants were considered: J_1 for the interaction between Mn1 and Mn2; J_2 for the exchange between Mn1 and both Mn3 and Mn4; J_3 for the coupling between Mn2 and both Mn3 and Mn4; and J_4 for the interaction between Mn3 and Mn4 (Figure 9). The g-value for the ions was fixed at 2.0, and any axial anisotropy

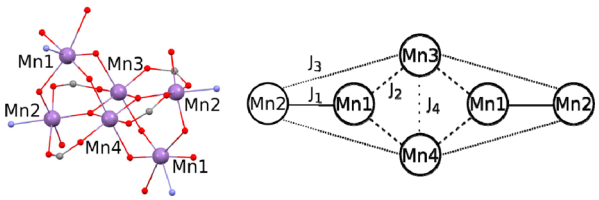

Figure 9. (left) View of the connectivity of the Mn(III) ions in **2**, and (right) a schematic of the exchange interactions used for the fitting process. For clarity, equivalent interactions are shown with the same type of lines.

associated with the six Mn(III) ions was omitted to reduce the number of parameters in the fit. The Hamiltonian used for the fit was as follows, where asterisks represent symmetry-equivalent sites.

$$\begin{aligned}\mathcal{H} = &-2\mathcal{J}_1(\hat{S}_1\hat{S}_2 + \hat{S}_{1*}\hat{S}_{2*}) + -2\mathcal{J}_2(\hat{S}_1\hat{S}_3 + \hat{S}_1\hat{S}_4 + \hat{S}_{1*}\hat{S}_3 \\ &+ \hat{S}_{1*}\hat{S}_4) + -2\mathcal{J}_3(\hat{S}_2\hat{S}_3 + \hat{S}_2\hat{S}_4 + \hat{S}_{2*}\hat{S}_3 + \hat{S}_{2*}\hat{S}_4) \\ &- 2\mathcal{J}_4(\hat{S}_3\hat{S}_4) + g\mu_B\vec{B}\sum_{i=1}^{6}\vec{s}_i \end{aligned} \quad (4)$$

The fit of $\chi_M T$ versus T yielded $J_1 = -5.99$ cm^{-1}; $J_2 = -2.40$ cm^{-1}; $J_3 = -11.09$ cm^{-1}; and $J_4 = -23.75$ cm^{-1} ($R = 99\%$). The strongest interaction is found between Mn3 and Mn4, consistent with data in the literature. The coupling in this type of butterfly arrangement, where Mn3 and Mn4 define the body and both Mn2 ions define the wings, is found to depend on the oxidation state of the ions in the wings.[59] When both ions in the wings are Mn(III), as is the case here, then the exchange between the two Mn(III) ions in the body is usually anti-ferromagnetic with values below -20 cm^{-1}.[60−64] The exchange interactions between Mn1 and Mn2, and between Mn1 and Mn3 and Mn4, all occur through monatomic alkoxido bridges. However, the Mn−O−Mn angle is different in the two cases, measuring 117.4(2)° for the angle between Mn1 and Mn2, and 121.4(2) and 122.8(2)° for the angles between Mn1 and Mn3, and Mn1 and Mn4, respectively. The distance between Mn1 and Mn2 (3.508 Å) is also significantly shorter than the distance between not only Mn1 and Mn3 (3.647 Å) but also Mn1 and Mn4 (3.626 Å). This could explain the stronger interaction J_1 between Mn1 and Mn2 compared to that between Mn1 and Mn3 and Mn4, J_2. For interatomic distances above 3.6 Å and Mn−O−Mn angles above 120°, the coupling has been found to be ca. -2 cm^{-1}, in line with that found here for J_2.[65] The coupling constant J_2 lies in the range of that found for other similarly connected Mn(III) ions in the literature.[64,66]

We also computed using DFT calculations the coupling constants in the hexanuclear complex **2**. They are presented in Table 2, and a good agreement between the theoretical and experimental values is observed, thus confirming the anti-ferromagnetic coupling constants J_1 to J_4 and giving reliability to the Hamiltonian used for the fitting and also the level of theory used for the calculations. The atomic spin density values of the Mn centers and the donor atoms of the ligands are summarized in Table S6 for the four pairwise magnetic coupling interactions. Moreover, the representation of the spin distribution corresponding to the high-spin state of complex **2** is plotted in Figure S10. The spin population values in the four [Mn$_2$] dimers reveal that most of the spin is carried by the Mn(III) magnetic centers and that the spin delocalization is

DOI: 10.1021/acs.inorgchem.6b02813
Inorg. Chem. XXXX, XXX, XXX−XXX

Table 2. Summary of the Experimental and Theoretical Magnetic Coupling Constants

compound	J	experimental[a]	theoretical[b]
1	J_1 (Mn^{III}–Mn^{II})	−5.95	−6.07
2	J_1 (Mn1–Mn2)	−5.99	−6.55
2	J_2 (Mn1–Mn3)	−2.40	−4.77
2	J_3 (Mn2–Mn3)	−11.09	−14.01
2	J_4 (Mn3–Mn4)	−23.75	−28.40

[a]Units of J, cm^{-1}. [b]B3LYP/6-31G*.

small (from 2.25% to 2.75% of the spin for the unpaired electrons on Mn(III) centers is delocalized to the ligand atoms, depending on the pairwise interaction). Remarkably, the spin carried by the alkoxido atom O6 is higher than O9, in agreement with the stronger interaction J_1 between Mn1 and Mn2 (via O6) compared to that between Mn1 and Mn3 (via O9), J_2. The spin population also reveals that the exchange interaction between Mn2 and Mn3 occurs through the carboxylate bridges.

Functional Activity for Catechol Oxidation. The catalytic oxidation behavior of complexes **1** and **2** were examined in aerobic conditions using 3,5-di-*tert*-butylcatechol (3,5-$DTBCH_2$) as a model prototypical catechol oxidase substrate. The *tert*-butyl substituents at the 3 and 5 positions of the aromatic ring makes the oxidation reaction feasible forming 3,5-di-*tert*-butylquinone (3,5-DTBQ) in MeOH and MeCN having absorption maxima at 401 and 403 nm, respectively. Solutions of complexes **1** and **2** ($\sim 1 \times 10^{-5}$ mol L^{-1}) were treated with 100 equiv ($\sim 1 \times 10^{-3}$ mol L^{-1}) of 3,5-$DTBCH_2$ under aerobic conditions in two different solvents (MeOH and MeCN), and time-dependent UV–vis spectra were recorded up to 1 h. Control experiments were performed using manganese(II) perchlorate and 100 equiv of $DTBCH_2$, where no change was observed in absorption intensity even after 1 d.

Oxidation in MeOH. Both **1** and **2** behave in a similar fashion during catalytic oxidation of $DTBCH_2$. Figure 10 shows the changes in spectral behavior of the two complexes on treatment with $DTBCH_2$. The oxidation reaction was followed for 1 h, after addition of the substrate $DTBCH_2$. Initially both the complexes show a broad absorption band centered at ∼405 nm in MeOH. After addition of $DTBCH_2$ the band instantly shifts to longer wavelength (∼430 nm for **1** and ∼413 nm for **2**) with the generation of a shoulder at ∼309 nm. On the one hand, as time passes, the former band gradually blue shifts and finally becomes stabilized at 404 and 402 nm for **1** and **2**, respectively. The shoulder at 309 nm, on the other hand, gradually disappears with the progress of the reaction with time. This observation of appearance and disappearance of the shoulder peak can be explained by taking into consideration the initial formation of a catalyst–substrate adduct, which decomposes with time upon generation of the stable oxidized product DTBQ.[67]

Oxidation in MeCN. The catalytic oxidation potency of **1** and **2** in air was studied and compared in MeCN medium to identify the solvent effect in the oxidation process. Upon treatment of **1**, having an absorption maximum at 392 nm, with 100 equiv of $DTBCH_2$, the intensity of maximum absorption increases significantly in favor of **1** to be identified as a catalyst for the aerobic oxidation of DTBC to DTBQ (Figure 11). The reaction was monitored by UV–vis spectro-photometry up to 1 h of time, showing saturation after 45 min of addition of $DTBCH_2$. Unlike the MeOH case, the MeCN medium did not show any additional absorption band characteristic of any complex–substrate aggregate, possibly due to the involvement of a fast kinetic process during the oxidation of 3,5-$DTBCH_2$ to 3,5-DTBQ. We also observed that complex **2** is catalytically inactive in MeCN medium. Initially complex **2** shows an absorption band at 409 nm, which upon addition of 3,5-$DTBCH_2$, registers a quenching in maxima at 411 nm. Most probably this is due to the weak interaction of **2** with the substrate molecule, that is, adduct formation in MeCN, not the expected oxidation behavior.

Kinetic Study for Catechol Oxidation. Kinetic evaluation for the oxidation of 3,5-$DTBCH_2$ in the presence of **1** and **2** was performed in MeOH for both **1** and **2** and in MeCN for **1** only. In all cases the complex solutions (fixed concentration ≈ 1×10^{-5} mol L^{-1}) were treated with varying concentrations of 3,5-DTBC (10 to 100 equiv). For all complex–substrate combinations, the formation of DTBQ was monitored by UV–vis spectrophotometry by recording the change in absorption intensity at 401 nm in MeOH and at 403 nm in MeCN within first 10 min of mixing. The reaction rates were calculated by initial rate method and were analyzed by the

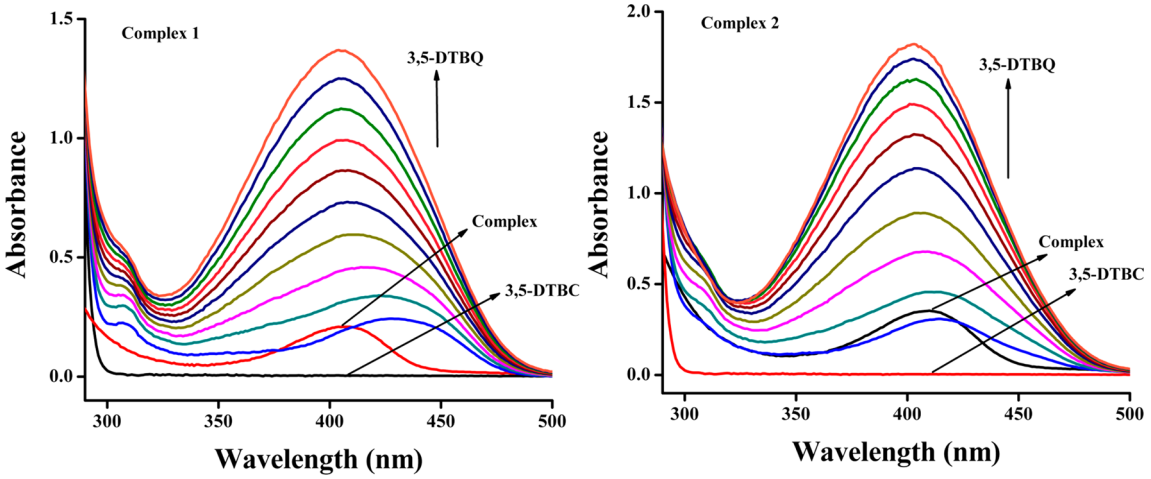

Figure 10. Time-dependent UV–vis spectral changes for **1** and **2** (concentration ≈ 1×10^{-5} mol L^{-1}) upon addition of excess (100-fold) 3,5-$DTBCH_2$ (concentration ≈ 1×10^{-3} mol L^{-1}) in MeOH at 298 K.

DOI: 10.1021/acs.inorgchem.6b02813
Inorg. Chem. XXXX, XXX, XXX–XXX

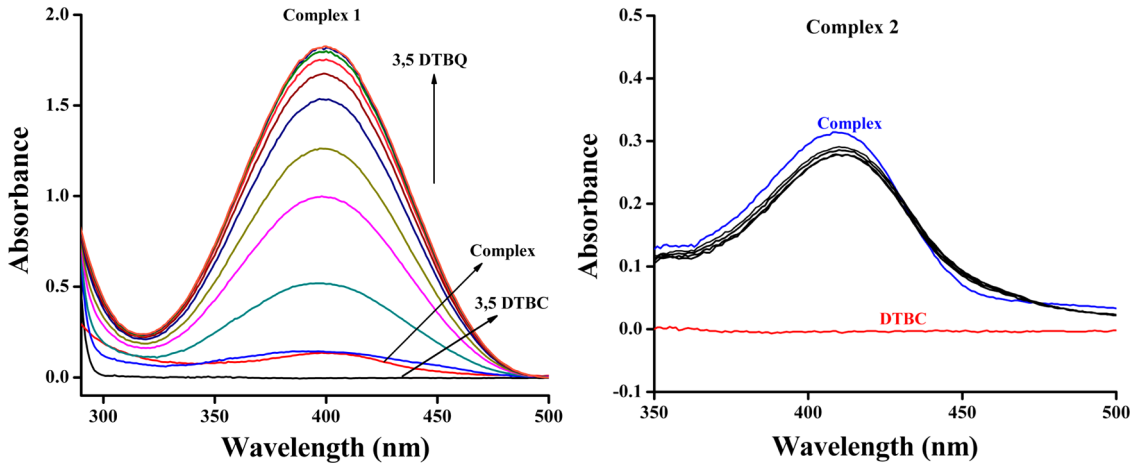

Figure 11. Time-dependent UV–vis spectra of complexes **1** and **2** (concentration ≈ 1×10^{-5} mol L^{-1}) after addition of excess (100-fold) 3,5-$DTBCH_2$ (concentration ≈ 1×10^{-3} mol L^{-1}) in MeCN at 298 K.

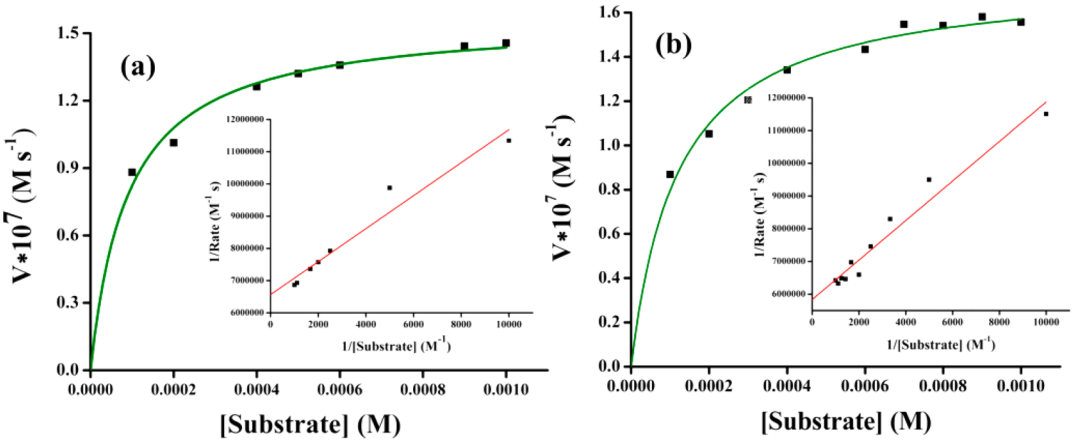

Figure 12. Dependence of the reaction rates on the substrate concentration for the oxidation of 3,5-$DTBCH_2$ catalyzed by complexes **1** (a) and **2** (b) in MeOH. The Lineweaver–Burk plots (inset).

Michaelis–Menten model of enzyme kinetics. In all cases the important kinetic parameters were extracted from the corresponding Lineweaver–Burk plots for all cases (Figures 12 and 13 insets). The kinetic parameters, such as the maximum reaction rate (V_{max}), the binding constant (K_M), and the turnover numbers (k_{cat}) for the oxidation reaction are listed in Table 3. The magnitude of K_M shows the concentration of the substrate when the reaction velocity is equal to one-half of the maximal velocity for the reaction. It can also be a measure of the binding affinity for the substrate. The observed kinetic parameters are comparable to that reported in the literature (Table S7).[68−72] Determination of turnover number (k_{cat}) of the metal complexes is important to understand their relative efficiency. The experiments for the detection of formed H_2O_2 in the reaction medium following iodometric method did not provide any proof in support of formation of I_2 in the medium, excluding the possibility of formation of H_2O_2 during the catalytic process.

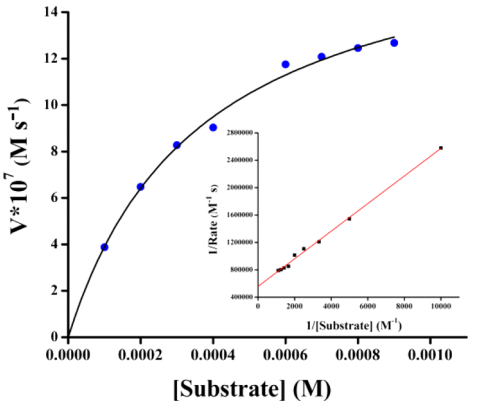

Figure 13. Dependence of the reaction rates on the substrate concentration for the oxidation of 3,5-$DTBCH_2$ catalyzed by **1** in MeCN. The Lineweaver–Burk plot (inset).

Mass Spectroscopic Analysis. To understand the nature of the fragments present in the two solvents used in this study and their dependence on the catalytic propensity, we scrutinized corresponding mass spectral patterns in MeOH and MeCN.

Fragments in MeOH. The mass spectrum (HRMS) of **1** (Figure S11) shows five peaks of medium-to-high intensity types at m/z values of 236.1284, 307.2021, 329.0687, 405.1249, and 523.1647. On the basis of the calculated m/z values these peaks can be assigned to the fragments $[hydrolyzed\text{-}H_2L1]H^+$ ($C_{13}H_{18}NO_3$; Calcd 236.1287), $[H_3L1\text{-}H]^+$ ($C_{17}H_{27}N_2O_3$; Calcd 307.2022), $[H_3L1\text{-}Na]^+$ ($C_{17}H_{26}N_2NaO_3$; Calcd 329.1841), $[Mn(hydrolyzed\text{-}HL1)(O_2CCH_3)(OH_2)\text{-}K]^+$ ($C_{15}H_{21}KMnNO_6$; Calc. 405.0386), and $[Mn(HL1)$-

DOI: 10.1021/acs.inorgchem.6b02813
Inorg. Chem. XXXX, XXX, XXX−XXX

Table 3. Kinetic Parameters for the Catalytic Oxidation of 3,5-DTBCH$_2$ by 1 and 2 at 25 °C

complex	solvent	V_{max} (M s^{-1})	K_M (M)	k_{cat} (h^{-1})	k_{cat}/K_M (s^{-1} M^{-1})
1	MeOH	(1.71 ± 0.05) × 10^{-7}	(1.04 ± 0.04) × 10^{-4}	61	162
2	MeOH	(1.52 ± 0.03) × 10^{-7}	(7.79 ± 0.49) × 10^{-5}	54	192
1	MeCN	(1.79 ± 0.05) × 10^{-6}	(3.44 ± 0.03) × 10^{-4}	644	520

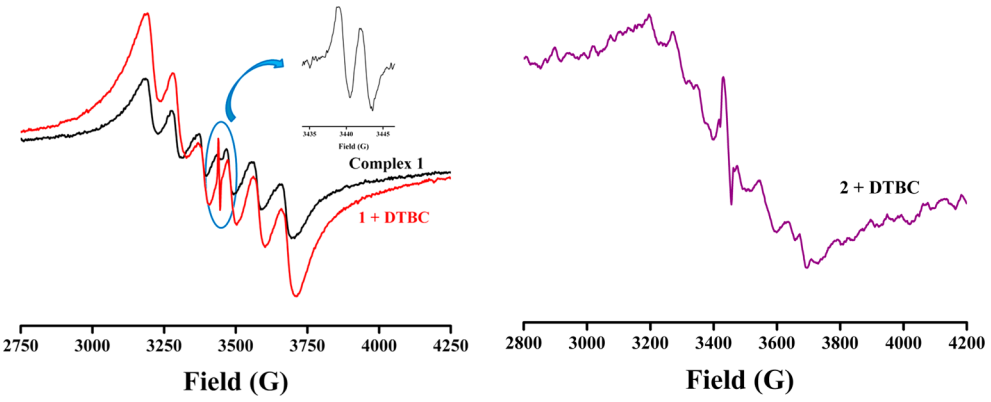

Figure 14. EPR spectra of 1 (black) and 1:100 mixtures (red and violet) of 1 and 2 with 3,5-DTBC in MeOH at room temperature.

$(O_2CCH_3)_2$-$Na_2]^+$ ($C_{21}H_{30}MnN_2Na_2O_7$; Calc. 523.1229), respectively. The mixture of 1 and 3,5-DTBCH$_2$ in 1:100 molar ratio was analyzed by electrospray ionization mass spectrometry (ESI MS) analysis after 10 min of mixing. The spectrum (Figure S12) shows characteristic peaks at 243.1381 and 463.2826 for [3,5-DTBQ-Na]$^+$ and [(3,5-DTBQ)$_2$-Na]$^+$, respectively. A less intense peak at m/z = 529.2846 is assigned to the catalyst−substrate aggregate [Mn(hydrolyzed-HL1)(3,5-DTSQH) (OH_2)]$^+$ ($C_{27}H_{40}MnNO_6$; Calc. 529.2236). The less intense peak at 543.3 can be assigned to the species [Mn(hydrolyzed-HL1) (DTBCH)(O_2)]$^+$ ($C_{27}H_{37}MnNO_7$, Calc 542.1951). The HRMS analysis of 2 in methanol (Figure S13) resulted in peaks at m/z = 266.1382, 367.2243, and 583.1844 from the fragments [H_3L3-H]$^+$ ($C_{14}H_{20}NO_4$; Calcd 266.1392), [Mn(L3) (OH_2) (CH_3OH)]$^+$ ($C_{15}H_{22}MnNO_6$; Calc. 367.0828), and [Mn_2(H_3L2)($O_2CC_2H_5$) (OH_2)$_2$]$^+$ ($C_{22}H_{37}Mn_2N_2O_9$; Calcd 583.1260) present in solution. The molecular ion peak corresponding to the formula [M]$^{2+}$ ($C_{78}H_{110}Mn_6N_6O_{28}$; Calcd m/z = 954.1825) appears at m/z = 954.1841. The HRMS (Figure S14) of 2 with added 3,5-DTBCH$_2$ (1:100) was recorded in MeOH solvent after 10 min of mixing. The spectrum provided a strong base peak at m/z = 243.1349 and a medium intense peak at 463.2826, for quinone-bearing fragments [3,5-DTBQ-Na]$^+$ and [(3,5-DTBQ)$_2$-Na]$^+$, respectively. The catalyst−substrate aggregate was detected at m/z = 353.2260 for [Mn(HL3)(3,5-DTBQ)-Na]$^+$ ($C_{28}H_{37}MnNNaO_6$; Calcd 561.1899). Another small peak at 705.4436 agrees to the fragment [Mn(H_2L3) (DTBCH)(O_2) (ClO_4) (CH_3OH)]H$^+$ ($C_{29}H_{44}ClMnNO_{13}$, Calc. 704.1882).

Fragments in MeCN. The HRMS spectra for 1 and 2 were also recorded in MeCN solution. In case of 1 (Figure S15), the peaks at m/z = 307.2017 and 329.0686 are assigned to the ligand associated with molecular formulas [H_3L1-H]$^+$ ($C_{17}H_{27}N_2O_3$; Calcd 307.2022) and [H_3L1-Na]$^+$ ($C_{17}H_{26}N_2NaO_3$; Calcd 329.1841). The presence of protonated hydrolyzed ligand [hydrolyzed-H_2L1-H]$^+$ ($C_{13}H_{18}NO_3$) was confirmed by the peak at m/z = 236.1301 (Calcd 236.1287). The mononuclear cationic molecular ion fragment [Mn-(hydrolyzed-HL1)(O_2CCH_3) (OH_2)-K]$^+$ ($C_{15}H_{21}KMnNO_6$) gave a peak at m/z = 405.1221 (Calc. 405.0386). The 1:100 mixture of 1 and 3,5-DTBC (after 10 min of mixing) resulted in two characteristic peaks at m/z = 243.1348 and 463.2815, respectively, for [DTBQ-Na]$^+$ and [(DTBQ)$_2$-Na]$^+$ (Figure S16). The characteristic peak for complex−substrate aggregate [Mn(H_2L1)(3,5-DTBC)-Na]$^+$ ($C_{31}H_{45}MnN_2O_5Na$) appeared as a small signal at m/z = 603.2462 (Calcd 603.2607). The peak at 543.3 corresponding to the O_2 bound fragment [Mn^{III}(hydrolyzed-HL1) (DTBCH)(O_2)]$^+$ in MeCN medium was also detected with certainty. Compound 2 in MeCN solution recorded a base peak at m/z = 367.2250 for the protonated ligand species [H_5L2-H]$^+$ ($C_{19}H_{31}N_2O_5$; Calcd 367.2233; Figure S17). Other peaks at m/z = 337.2132, 419.1398, and 806.1134 were assigned to the cationic molecular fragments [Mn(H_2L3) (OH_2)]$^+$ ($C_{14}H_{20}MnNO_5$; Calcd 337.0722), [Mn(H_3L2)]$^+$ ($C_{19}H_{28}MnN_2O_5$; Calcd 419.1379), and [Mn_3(L2)($O_2CC_2H_5$)$_3$($NCCH_3$) (OH_2)]$^+$ ($C_{30}H_{45}Mn_3N_3O_{12}$; Calcd 804.1145).

Thus, the ESI-MS spectra allow us to conclude that the complex−substrate intermediates are formed during oxidation reactions of DTBCH$_2$ to 3,5-DTBQ by O_2 of air. The analysis also established that the ligand/hydrolyzed-ligand bound mononuclear fragments are the catalytically active species in both the cases. The catalytic activity was not observed in case of 2 in MeCN due to nonavailability of the active mononuclear fragment in MeCN medium.

Probable Mechanism. Studied reaction kinetics showed that both complexes were reactive for simulating the catechol oxidase activity, and the rate saturation kinetics indicate that the oxidation reaction proceeds smoothly through a stable complex−substrate intermediate as observed for some mononuclear manganese(II) complexes.[67] Solution-phase EPR spectral measurements were performed to comment on the catalytic pathways for the oxidation reactions. In MeOH, separate mixtures of 1 and 2 with DTBC (1:100) in methanol solution were examined following the recorded EPR spectra. Complex 1, containing one Mn^{II}, generated hyperfine sextet (six-line) EPR spectra with g values of 2.14, 2.09, 2.03, 1.97, 1.92, and 1.87 and A_{av} value of 93.2 G. The six hyperfine lines are due to the interaction of the electron spin with the nuclear spin (^{55}Mn, I = 5/2).[73] Interestingly, upon addition of 100

DOI: 10.1021/acs.inorgchem.6b02813
Inorg. Chem. XXXX, XXX, XXX−XXX

equiv of the substrate to the solutions of **1**, the intensity of six-line hyperfine splitting pattern in the spectrum is increased, which suggests that the concentration of manganese(II) species is increased several-fold after addition of the substrate (Figure 14). The spectrum also allowed us to detect the presence of an organic radical at g = 2.009 following the conversion of DTBC to DTBQ in radical pathway. Expanded scan in the region showed further splitting into two lines (a_{av}, 3.09 G). Similarly, complex **2**, which is silent in present working mode of EPR (perpendicular mode), also indicated the conversion of DTBC to DTBQ from sextet EPR lines originating from the reaction generated Mn^{II} along with signal for the organic radical. From the combined ESI-MS and EPR spectra analysis a plausible mechanistic pathway is proposed in Scheme S2.

CONCLUSION

Trinuclear and hexanuclear manganese complexes have been presented from unusual binding of ligands having dangling and hydrolyzed arms. Two closely related binucleating ligands have been used for mixed-valent linear $Mn^{III}_2Mn^{II}$ and fused diadamantane-type Mn^{III}_6 coordination aggregates in **1** and **2**. The study also examined the relative stability of the imine functions not utilized for coordination to manganese ions. Very unusual binding modes and coordination from terminal alcohol ends of the ligands were observed during the growth of such multimetallic assemblies. In MeOH reaction medium the externally added carboxylates and in situ generated hydroxido groups were involved in competitive metal ion binding for the growth of aggregates. The work also establishes the coordination flexibility and bridging preference of the used ligands. The deprotonated phenol part and protonated as well as deprotonated alcohol ends were utilized for the growth of new manganese aggregates of varying nuclearity and contrasting molecular topology. The intramolecular exchange interactions in **1** and **2** are anti-ferromagnetic in nature. For **1**, the magnetic susceptibility and magnetization data were fitted simultaneously using one coupling constant and the single-ion axial magnetic anisotropy on the two Mn(III) centers. The ac data showed that **1** displayed a field-induced slow magnetic relaxation at 2 K. For **2**, in the fit of $\chi_M T$ versus T four different coupling constants were justified in the accordance with the different Mn···Mn interactions and found to be in good agreement with DFT calculations. Both complexes exhibit catecholase-like activity toward 3,5-DTBCH$_2$ as the model substrate with comparable catalytic efficiency with a pronounced solvent effect in case of the former. Kinetic studies on the solvent-dependent oxidation reaction of 3,5-di-*tert*-butylcatechol by O_2 in solution establish both the trinuclear and hexanuclear complexes as efficient catalysts in MeOH. In MeCN medium, complex **2** is inactive. ESI-MS (positive) proofs clearly advocate the presence of mononuclear manganese complex−catechol collections and bidentate coordination mode of catechol unit undergoing oxidation.

ASSOCIATED CONTENT

Supporting Information

The Supporting Information is available free of charge on the ACS Publications website at DOI: 10.1021/acs.inorgchem.6b02813.

FTIR spectra, electronic spectra, illustrated aggregation process, illustrated H-bonded framework in complex **1**, additional illustrations of complexes, plotted ac susceptibility measurements, illustrated mechanistic pathway for oxidation of substituted catechol, ESI-MS spectra, tabulated crystallographic data, selected bond distances and bond angles in complexes **1** and **2**, hydrogen-bonding parameters, bond valence sums, calculated Mulliken spin population (PDF)

X-ray crystallographic data in CIF format, CCDC Nos. 1517620 and 1517621 contain the supplementary crystallographic data in CIF format for complexes **1** and **2** (ZIP)

AUTHOR INFORMATION

Corresponding Author

*E-mail: dray@chem.iitkgp.ernet.in. Tel: (+91) 3222-283324. Fax: (+91) 3222-82252.

ORCID

Debashis Ray: 0000-0002-4174-6445

Notes

The authors declare no competing financial interest.

ACKNOWLEDGMENTS

K.C. is thankful to the Council of Scientific and Industrial Research, New Delhi, for the financial support. K.C. is thankful to Dr. D. Banerjee for his kind help in collecting EPR data. We are also thankful to DST, New Delhi, for providing the Single Crystal X-ray Diffractometer facility to the Dept. of Chemistry, IIT Kharagpur, under its FIST program. A.F. thanks the DGICYT of Spain (Project No. CTQ2014-57393-C2-1-P, FEDER funds). We thank the CTI (UIB) for computational facilities. We are thankful to the reviewers for their valuable suggestions to improve the quality of the manuscript.

REFERENCES

(1) Hoffman, B. M.; Dean, D. R.; Seefeldt, L. C. Climbing nitrogenase: toward a mechanism of enzymatic nitrogen fixation. *Acc. Chem. Res.* **2009**, *42*, 609−619.

(2) Zouni, A.; Witt, H. T.; Kern, J.; Fromme, P.; Krauss, N.; Saenger, W.; Orth, P. Crystal structure of photosystem II from Synechococcus elongatus at 3.8 Å resolution. *Nature* **2001**, *409*, 739−743.

(3) Kamiya, N.; Shen, J. R. Crystal structure of oxygen-evolving photosystem II from Thermosynechococcus vulcanus at 3.7-Å resolution. *Proc. Natl. Acad. Sci. U. S. A.* **2003**, *100*, 98−103.

(4) Ferreira, K. N.; Iverson, T. M.; Maghlaoui, K.; Barber, J.; Iwata, S. Architecture of the photosynthetic oxygen-evolving center. *Science* **2004**, *303*, 1831−1838.

(5) Biesiadka, J.; Loll, B.; Kern, J.; Irrgang, K. D.; Zouni, A. Crystal structure of cyanobacterial photosystem II at 3.2 Å resolution: a closer look at the Mn-cluster. *Phys. Chem. Chem. Phys.* **2004**, *6*, 4733−4736.

(6) Carrell, T.; Tyryshkin, A.; Dismukes, G. An evaluation of structural models for the photosynthetic water-oxidizing complex derived from spectroscopic and X-ray diffraction signatures. *JBIC, J. Biol. Inorg. Chem.* **2002**, *7*, 2−22.

(7) Cinco, R. M.; Rompel, A.; Visser, H.; Aromí, G.; Christou, G.; Sauer, K.; Klein, M. P.; Yachandra, V. K. Comparison of the manganese cluster in oxygen-evolving photosystem II with distorted cubane manganese compounds through X-ray absorption spectroscopy. *Inorg. Chem.* **1999**, *38*, 5988−5998.

(8) Yachandra, V. K.; Sauer, K.; Klein, M. P. Manganese cluster in photosynthesis: where plants oxidize water to dioxygen. *Chem. Rev.* **1996**, *96*, 2927−2950.

(9) Bagai, R.; Abboud, K. A.; Christou, G. Ligand-induced distortion of a tetranuclear manganese butterfly complex. *Dalton Trans.* **2006**, 3306−3312.

(10) Hamilton, C. R.; Gau, M. R.; Baglia, R. A.; McWilliams, S. F.; Zdilla, M. J. Mechanistic Elucidation of the stepwise formation of a

DOI: 10.1021/acs.inorgchem.6b02813
Inorg. Chem. XXXX, XXX, XXX−XXX

tetranuclear manganese pinned butterfly cluster via N−N bond cleavage, hydrogen atom transfer, and cluster rearrangement. *J. Am. Chem. Soc.* **2014**, *136*, 17974−17986.
(11) Yang, H.; Cao, F.; Li, D.; Zeng, S.; Song, Y.; Dou, J. Solvent dependent reactivities of di-, tetra-and hexanuclear manganese complexes: syntheses, structures and magnetic properties. *Dalton Trans.* **2015**, *44*, 6620−6629.
(12) Elshaarawy, R. F. M.; Lan, Y.; Janiak, C. Oligonuclear homo- and mixed-valence manganese complexes based on thiophene- or aryl-carboxylate ligation: Synthesis, characterization and magnetic studies. *Inorg. Chim. Acta* **2013**, *401*, 85−94.
(13) Ledesma, G. N.; Anxolabéhère-Mallart, E.; Rivière, E.; Mallet-Ladeira, S.; Hureau, C.; Signorella, S. R. Trinuclear manganese complexes of unsymmetrical polypodal diamino N_3O_3 ligands with an unusual $[Mn_3(\mu\text{-}OR)_4]^{5+}$ triangular core: synthesis, characterization, and catalase activity. *Inorg. Chem.* **2014**, *53*, 2545−2553.
(14) Ghosh, A. K.; Shatruk, M.; Bertolasi, V.; Pramanik, K.; Ray, D. Self-assembled tetra-and pentanuclear nickel(II) aggregates from phenoxido-based ligand-bound $\{Ni_2\}$ fragments: carboxylate bridge controlled structures. *Inorg. Chem.* **2013**, *52*, 13894−13903.
(15) Adhikary, J.; Chakraborty, A.; Dasgupta, S.; Chattopadhyay, S. K.; Kruszynski, R.; Trzesowska-Kruszynska, A.; Stepanović, S.; Gruden-Pavlović, M.; Swart, M.; Das, D. Unique mononuclear Mn^{II} complexes of an end-off compartmental Schiff base ligand: experimental and theoretical studies on their bio-relevant catalytic promiscuity. *Dalton Trans.* **2016**, *45*, 12409−12422.
(16) Chakraborty, P.; Majumder, I.; Banu, K. S.; Ghosh, B.; Kara, H.; Zangrando, E.; Das, D. Mn(II) complexes of different nuclearity: synthesis, characterization and catecholase-like activity. *Dalton Trans.* **2016**, *45*, 742−752.
(17) Milios, C. J.; Manoli, M.; Rajaraman, G.; Mishra, A.; Budd, L. E.; White, F.; Parsons, S.; Wernsdorfer, W.; Christou, G.; Brechin, E. K. A family of $[Mn_6]$ complexes featuring tripodal ligands. *Inorg. Chem.* **2006**, *45*, 6782−6793.
(18) Sawada, Y.; Kosaka, W.; Hayashi, Y.; Miyasaka, H. Coulombic aggregations of Mn^{III} salen-type complexes and Keggin-type polyoxometalates: isolation of Mn_2 single-molecule magnets. *Inorg. Chem.* **2012**, *51*, 4824−4832.
(19) Martínez-Lillo, J.; Tomsa, A.-R.; Li, Y.; Chamoreau, L.-M.; Cremades, E.; Ruiz, E.; Barra, A.-L.; Proust, A.; Verdaguer, M.; Gouzerh, P. Synthesis, crystal structure and magnetism of new salicylamidoxime-based hexanuclear manganese (III) single-molecule magnets. *Dalton Trans.* **2012**, *41*, 13668−13681.
(20) Zhang, L.; Onet, C. I.; Clérac, R.; Rouzières, M.; Marzec, B.; Boese, M.; Venkatesan, M.; Schmitt, W. A facile "bottom-up" approach to prepare free-standing nano-films based on manganese coordination clusters. *Chem. Commun.* **2013**, *49*, 7400−7402.
(21) Wang, P.; Yap, G. P. A.; Riordan, C. G. Five-coordinate M^{II}-semiquinonate (M = Fe, Mn, Co) complexes: reactivity models of the catechol dioxygenases. *Chem. Commun.* **2014**, *50*, 5871−5873.
(22) Dey, S. K.; Mukherjee, A. The synthesis, characterization and catecholase activity of dinuclear cobalt (II/III) complexes of an O-donor rich Schiff base ligand. *New J. Chem.* **2014**, *38*, 4985−4995.
(23) Biswas, A.; Das, L. K.; Drew, M. G. B.; Aromí, G.; Gamez, P.; Ghosh, A. Synthesis, crystal structures, magnetic properties and catecholase activity of double phenoxido-bridged penta-coordinated dinuclear nickel (II) complexes derived from reduced Schiff-base ligands: mechanistic inference of catecholase activity. *Inorg. Chem.* **2012**, *51*, 7993−8001.
(24) Pait, M.; Bauza, A.; Frontera, A.; Colacio, E.; Ray, D. A new family of Ni_4 and Ni_6 aggregates from the self-assembly of $[Ni_2]$ building units: role of carboxylate and carbonate bridges. *Inorg. Chem.* **2015**, *54*, 4709−4723.
(25) Dhara, K.; Saha, U. C.; Dan, A.; Sarkar, S.; Manassero, M.; Chattopadhyay, P. A new water−soluble copper (II) complex as a selective fluorescent sensor for azide ion. *Chem. Commun.* **2010**, *46*, 1754−1756.
(26) Gagne, R. R.; Spiro, C. L.; Smith, T. J.; Hamann, C. A.; Thies, W. R.; Shiemke, A. K. The synthesis, redox properties, and ligand binding of heterobinuclear transition-metal macrocyclic ligand complexes. Measurement of an apparent delocalization energy in a mixed-valent copper(I) copper(II) complex. *J. Am. Chem. Soc.* **1981**, *103*, 4073−4081.
(27) *Saint, Smart and XPREP;* Siemens Analytical X-ray Instruments Inc.: Madison, WI, 1995.
(28) Sheldrick, G. M. *SHELXS-97;* Universityof Göttingen: Göttingen, Germany, 1997.
(29) Sheldrick, G. M. *SHELXL 97,* Program for Crystal Structure Refinement; University of Göttingen: Göttingen, Germany, 1997.
(30) Farrugia, L. *WinGX System,* v. 1.80.05; University of Glasgow: U.K., 2017.
(31) *DIAMOND,* Visual Crystal Structure Information System, version 3.1; Crystal Impact: Bonn, Germany, 2004.
(32) Farrugia, L. J. *POV-Ray 3.5;* Glasgow University: Australia, 2003.
(33) Noodleman, L. J. Valence bond description of antiferromagnetic coupling in transition metal dimers. *J. Chem. Phys.* **1981**, *74*, 5737−5743.
(34) Noodleman, L.; Davidson, E. R. Ligand spin polarization and antiferromagnetic coupling in transition metal dimers. *Chem. Phys.* **1986**, *109*, 131−143.
(35) Noodleman, L.; Peng, C. Y.; Case, D. A.; Mouesca, J. M. Orbital interactions, electron delocalization and spin coupling in iron-sulfur clusters. *Coord. Chem. Rev.* **1995**, *144*, 199−244.
(36) Frisch, M. J.; Trucks, G. W.; Schlegel, H. B.; Scuseria, G. E.; Robb, M. A.; Cheeseman, J. R.; Scalmani, G.; Barone, V.; Mennucci, B.; Petersson, G. A.; Nakatsuji, H.; Caricato, M.; Li, X.; Hratchian, H. P.; Izmaylov, A. F.; Bloino, J.; Zheng, G.; Sonnenberg, J. L.; Hada, M.; Ehara, M.; Toyota, K.; Fukuda, R.; Hasegawa, J.; Ishida, M.; Nakajima, T.; Honda, Y.; Kitao, O.; Nakai, H.; Vreven, T.; Montgomery, J. A., Jr.; Peralta, J. E.; Ogliaro, F.; Bearpark, M.; Heyd, J. J.; Brothers, E.; Kudin, K. N.; Staroverov, V. N.; Kobayashi, R.; Normand, J.; Raghavachari, K.; Rendell, A.; Burant, J. C.; Iyengar, S. S.; Tomasi, J.; Cossi, M.; Rega, N.; Millam, J. M.; Klene, M.; Knox, J. E.; Cross, J. B.; Bakken, V.; Adamo, C.; Jaramillo, J.; Gomperts, R.; Stratmann, R. E.; Yazyev, O.; Austin, A. J.; Cammi, R.; Pomelli, C.; Ochterski, J. W.; Martin, R. L.; Morokuma, K.; Zakrzewski, V. G.; Voth, G. A.; Salvador, P.; Dannenberg, J. J.; Dapprich, S.; Daniels, A. D.; Farkas, Ö.; Foresman, J. B.; Ortiz, J. V.; Cioslowski, J.; Fox, D. J. *Gaussian 09,* Revision D.01; Gaussian, Inc.: Wallingford, CT, 2009.
(37) Costa, R.; Valero, R.; Mañeru, D. R.; Moreira, I. de P. R.; Illas, F. Spin adapted versus broken symmetry approaches in the description of magnetic coupling in heterodinuclear complexes. *J. Chem. Theory Comput.* **2015**, *11*, 1006−1019.
(38) Reta Mañeru, D.; Costa, R.; Guix Márquez, M.; Moreira, I. de P. R.; Illas, F. Handling magnetic coupling in trinuclear Cu (II) complexes. *J. Chem. Theory Comput.* **2015**, *11*, 3650−3660.
(39) Ruiz, E.; Rodríguez-Fortea, A.; Cano, J.; Alvarez, S.; Alemany, P. About the calculation of exchange coupling constants in polynuclear transition metal complexes. *J. Comput. Chem.* **2003**, *24*, 982−989.
(40) Ruiz, E.; Alvarez, S.; Cano, J.; Polo, V. About the calculation of exchange coupling constants using density-functional theory: The role of the self-interaction error. *J. Chem. Phys.* **2005**, *123*, 164110−164117.
(41) Mandal, D.; Bertolasi, V.; Ribas-Ariño, J.; Aromí, G.; Ray, D. Self-Assembly of an Azido-Bridged $[Ni^{II}_6]$ Cluster Featuring Four Fused Defective Cubanes. *Inorg. Chem.* **2008**, *47*, 3465−3467.
(42) Liu, W.; Thorp, H. H. Bond valence sum analysis of metal-ligand bond lengths in metalloenzymes and model complexes. 2. Refined distances and other enzymes. *Inorg. Chem.* **1993**, *32*, 4102−4105.
(43) Brown, I. D. Recent developments in the methods and applications of the bond valence model. *Chem. Rev.* **2009**, *109*, 6858−6919.
(44) Tandon, S. S.; Bunge, S. D.; Sanchiz, J.; Thompson, L. K. Structures and magnetic properties of an antiferromagnetically coupled polymeric copper(II) complex and ferromagnetically coupled hexanuclear nickel(II) clusters. *Inorg. Chem.* **2012**, *51*, 3270−3282.
(45) Ma, Y. S.; Yao, H. C.; Hua, W. J.; Li, S. H.; Li, Y. Z.; Zheng, L. M. Tetranuclear manganese (III) clusters containing both carboxylate

DOI: 10.1021/acs.inorgchem.6b02813
Inorg. Chem. XXXX, XXX, XXX−XXX

and phosphonate bridging ligands. *Inorg. Chim. Acta* **2007**, *360*, 1645−1650.
(46) Libby, E.; McCusker, J. K.; Schmitt, E. A.; Folting, K.; Hendrickson, D. N.; Christou, G. Preparation and properties of models for the photosynthetic water oxidation center: spin frustration in the manganese $[Mn_4O_2\ (O_2CR)_7(pic)_2]$-anion. *Inorg. Chem.* **1991**, *30*, 3486−3495.
(47) Aromí, G.; Bhaduri, S.; Artús, P.; Folting, K.; Christou, G. Bridging nitrate groups in $[Mn_4O_3(NO_3)(O_2CMe)_3\ (R_2dbm)_3]$(R= H, Et) and $[Mn_4O_2(NO_3)(O_2CEt)_6(bpy)_2](ClO_4)$: acidolysis routes to tetranuclear manganese carboxylate complexes. *Inorg. Chem.* **2002**, *41*, 805−817.
(48) Escuer, A.; Mayans, J.; Font-Bardia, M. Copper(II) cubanes with a {Cu4O} core and well defined S = 1 ground state. *Dalton Trans.* **2016**, *45*, 1604−1613.
(49) Pait, M.; Colacio, E.; Ray, D. Novel anion-tunable structural diversity and new topologies in Cu^{II} complexes of a Schiff base. *Polyhedron* **2015**, *88*, 90−100.
(50) Milios, C. J.; Inglis, R.; Vinslava, A.; Bagai, R.; Wernsdorfer, W.; Parsons, S.; Perlepes, S. P.; Christou, G.; Brechin, E. K. *J. Am. Chem. Soc.* **2007**, *129*, 12505−12511.
(51) Taguchi, T.; Daniels, M. R.; Abboud, K. A.; Christou, G. Mn_4, Mn_6 and Mn_{11} clusters from the use of bulky diphenyl(pyridine-2-yl)methanol. *Inorg. Chem.* **2009**, *48*, 9325−9335.
(52) Stamatatos, T. C.; Luisi, B. S.; Moulton, B.; Christou, G. Employment of 2,6-diacetylpyridine dioxime as a new route to high nuclearity metal clusters: Mn_6 and Mn_8 complexes. *Inorg. Chem.* **2008**, *47*, 1134−1144.
(53) Chilton, N. F.; Anderson, R. P.; Turner, L. D.; Soncini, A.; Murray, K. S. PHI: A powerful new program for the analysis of anisotropic monomeric and exchange-coupled polynuclear d-and f-block complexes. *J. Comput. Chem.* **2013**, *34*, 1164−1174.
(54) Pait, M.; Shatruk, M.; Ray, D. Anion coordination selective $[Mn_3]$ and $[Mn_4]$ assemblies: Synthesis, structural diversity, magnetic properties and catechol oxidase activity. *Dalton Trans.* **2015**, *44*, 11741−11754.
(55) Kessissoglou, D. P.; Kirk, M. L.; Lah, M. S.; Li, X.; Raptopoulou, C.; Hatfield, W. E.; Pecoraro, V. L. Structural and magnetic characterization of trinuclear, mixed-valence manganese acetates. *Inorg. Chem.* **1992**, *31*, 5424−5432.
(56) Boča, R. *A Handbook of Magnetochemical Formulae;* Elsevier Inc., 2012.
(57) Tziotzi, T. G.; Philippidis, A.; Raptopoulou, C. P.; Psycharis, V.; Milios, C. J. Employment of a naphthalene-based tetraol ligand in Mn chemistry: Mononuclear and linear trinuclear clusters. *Polyhedron* **2013**, *64*, 52−58.
(58) Duboc, C. Determination and prediction of the magnetic anisotropy of Mn ions. *Chem. Soc. Rev.* **2016**, *45*, 5834−5847.
(59) Wemple, M. W.; Tsai, H.-L.; Wang, S.; Claude, J. P.; Streib, W. E.; Huffman, J. C.; Hendrickson, D. N.; Christou, G. Tetranuclear and octanuclear manganese carboxylate clusters: preparation and reactivity of $(NBu^n_4)[Mn_4O_2(O_2CPh)_9(H_2O)]$ and synthesis of $(NBu^n_4)_2[Mn_8O_4(O_2CPh)_{12}(Et_2mal)_2(H_2O)_2]$ with a "Linked-Butterfly" structure. *Inorg. Chem.* **1996**, *35*, 6437−6449.
(60) Kanady, J. S.; Tran, R.; Stull, J. A.; Lu, L.; Stich, T. A.; Day, M. W.; Yano, J.; Britt, R. D.; Agapie, T. Role of oxido incorporation and ligand lability in expanding redox accessibility of structurally related Mn_4 clusters. *Chem. Sci.* **2013**, *4*, 3986−3996.
(61) Aromí, G.; Bhaduri, S.; Artús, P.; Huffman, J. C.; Hendrickson, D. N.; Christou, G. A tetranuclear manganese carboxylate cluster with bis(2-pyridyl)amine ligation: $[Mn_4O_2(O_2CEt)_7(bpya)_2](ClO_4)$. *Polyhedron* **2002**, *21*, 1779−1786.
(62) Albela, B.; El Fallah, M. S.; Ribas, J.; et al. Two new mixed-valence manganese complexes of formula $[Mn_4O_2(X\text{-benzoato})_7(bpy)_2]$ (X = 2-Cl, 2-Br) and the crystal structure of the 2-Cl complex: Ground-state spin variability in the $[Mn_4O_2]^{7+}$ complexes. *Inorg. Chem.* **2001**, *40*, 1037−1044.
(63) Wang, S.; Wemple, M. S.; Yoo, J.; Folting, K.; Huffman, J. C.; Hagen, K. S.; Hendrickson, D. N.; Christou, G. Tetranuclear manganese carboxylate complexes with a trigonal pyramidal metal topology via controlled potential electrolysis. *Inorg. Chem.* **2000**, *39*, 1501−1513.
(64) Christmas, C.; Vincent, J. B.; Chang, H. R.; Huffman, J. C.; Christou, G.; Hendrickson, D. N. Nonanuclear oxide-bridged manganese complex. Preparation, structure, and magnetic properties of $[Mn_9O_4(O_2CPh)_8(sal)_4(salH)_2(pyr)_4]$ ($salH_2$ = salicylic acid; pyr = pyridine). *J. Am. Chem. Soc.* **1988**, *110*, 823−830.
(65) Yang, P.-P.; Song, X.-Y.; Liu, R.-N.; Li, L.-C.; Liao, D.-Z. Syntheses, crystal structures and magnetic properties of a novel family of penta-manganese complexes derived from an assembly system containing polydentate hydroxy-rich Schiff-base ligands. *Dalton Trans.* **2010**, *39*, 6285−6294.
(66) Shanmugam, M.; Shanmugam, M.; Chastanet, G.; Sessoli, R.; Mallah, T.; Wernsdorfer, W.; Winpenny, R. E. P. Minor changes in phosphonate ligands lead to new hexa-and dodeca-nuclear Mn clusters. *J. Mater. Chem.* **2006**, *16*, 2576−2578.
(67) Banu, K. S.; Chattopadhyay, T.; Banerjee, A.; Mukherjee, M.; Bhattacharya, S.; Patra, G. K.; Zangrando, E.; Das, D. Mono-and dinuclear manganese(III) complexes showing efficient catechol oxidase activity: syntheses, characterization and spectroscopic studies. *Dalton Trans.* **2009**, *40*, 8755−8764.
(68) Majumder, A.; Goswami, S.; Batten, S. R.; Salah El Fallah, M.; Ribas, J.; Mitra, S. Catalytic oxidation of 3,5-di-tert-butylcatechol by a manganese(III) 18-azametallacrown-6 compound: Synthesis, crystal structure, fluorescence, magnetic and kinetic investigation. *Inorg. Chim. Acta* **2006**, *359*, 2375−2382.
(69) Hitomi, Y.; Ando, A.; Matsui, H.; Ito, T.; Tanaka, T.; Ogo, S.; Funabiki, T. Aerobic catechol oxidation catalyzed by a bis(μ-oxo)dimanganese(III,III) complex via a manganese(II)-semiquinonate complex. *Inorg. Chem.* **2005**, *44*, 3473−3478.
(70) Triller, M. U.; Pursche, D.; Hsieh, W. Y.; Pecoraro, V. L.; Rompel, A.; Krebs, B. Catalytic oxidation of 3,5-di-tert-butylcatechol by a series of mononuclear manganese complexes: synthesis, structure, and kinetic investigation. *Inorg. Chem.* **2003**, *42*, 6274−6283.
(71) Jana, A.; Aliaga-Alcalde, N.; Ruiz, E.; Mohanta, S. Structures, magnetochemistry, spectroscopy, theoretical study, and catechol oxidase activity of dinuclear and dimer-of-dinuclear mixed-valence $Mn^{III}Mn^{II}$ complexes derived from a macrocyclic ligand. *Inorg. Chem.* **2013**, *52*, 7732−7746.
(72) Kar, P.; Ida, Y.; Kanetomo, T.; Drew, M. G. B.; Ishida, T.; Ghosh, A. Synthesis of mixed-valence hexanuclear Mn(II/III) clusters from its Mn(II) precursor: variations of catecholase-like activity and magnetic coupling. *Dalton Trans.* **2015**, *44*, 9795−9804.
(73) Garribba, E.; Micera, G. Determination of the hyperfine coupling constant and zero-field splitting in the ESR spectrum of Mn^{2+} in calcite. *Magn. Reson. Chem.* **2006**, *44*, 11−19.

DOI: 10.1021/acs.inorgchem.6b02813
Inorg. Chem. XXXX, XXX, XXX−XXX